

# 9. Adaptive Zones and the Pinniped Ankle: A Three-Dimensional Quantitative Analysis of Carnivoran Tarsal Evolution

P. David Polly\*  
*Department of Geological Sciences*  
*Indiana University*  
*1001 East 10th Street*  
*Bloomington, IN 47405, USA*  
*pdpolly@indiana.edu*

## 9.1 Introduction

*History repeats the old conceits, the glib replies, the same defeats*  
Elvis Costello (1982), *Beyond Belief*

Bones are functional. Stated so abruptly, this observation is a truism, but its significance depends on the context in which it is made. In an individual animal, bones support loads, resist muscular contractions, and facilitate bodily movements. Bone form both constrains, and is shaped by, force and motion. In an environmental context, a bone's form is compatible with its owner's size and habits and is, thus, related indirectly to habitat and environment, although any particular bone (or, more properly, musculoskeletal configuration) can cope in diverse environments, and any substrate can be traversed by animals with different skeletal forms. Form and function are inseparable at the level of joint movements (Bock and von Wahlert, 1965), but they are only loosely correlated at the level of ecology, specifically locomotor types and habitats. The coarseness of the correlation between form and ecology come from the temporal lag of phylogenetic adaptation and the many-to-many relationship between form and habitat. Even though ecophenotypic plasticity allows bones to be modified during an individual's lifetime, bone form is largely heritable and evolutionary change requires generations of selective genetic and epigenetic reorganization (Cock, 1966; Grüneberg, 1967; Thorpe, 1981).

Some have argued that functional adaptation is incompatible with phylogenetic reconstruction. Assertions as to whether skeletal variation is primarily phylogenetic (Acero et al., 2005) or functional (Nadal-Roberts and Collard, 2005) color the entire canon of systematic literature, but the nature of the conflict is murky – functional adaptation is a phylogenetic process and the

phylogenetic transformation of bone form does not occur outside a functional context. On one hand, all adaptive specializations, even those shared by different clades, arise phylogenetically, but on the other, no bone character is functionally neutral. The question, then, is not whether skeletal characters are functional – they are – but to what extent adaptation masks phylogenetic history, how the convergences can be recognized, whether adaptation impedes phylogeny reconstruction, and how the interplay between form, function, and phylogeny can be better understood. These questions are the main subject of this paper.

In this paper, function and phylogeny were analyzed using a new geometric morphometric technique that quantitatively represents the entire three-dimensional surface of the bones. This method was used to associate variation in the two bones, including the size and curvature of occluding joint facets, with locomotor type, stance, number of digits, and body mass. Principal components analysis was used to describe the major axes of variation in the two bones, and multivariate analysis of variance was used to test functional categories for significance. Correlated transformations in the interlocking surfaces of the two bones were also explored using two-block partial least squares. Phylogenetic components of variation were assessed by mapping the three-dimensional shape of the bones onto a cladogram and projecting the results back into the principal component morphospace to visualize the patterns of homoplasy. Rates of morphological evolution in the several clades were calculated from the mapped shapes. Homoplasy was also quantitatively assessed by measuring the scaling coefficient between evolutionary divergence and time since common ancestry. The final aim of this paper was to develop criteria for assessing the whether functional adaptation is likely to confound phylogenetic signal in a dataset for the taxa being considered. A quantitative redefinition of Simpson's adaptive zones was employed to assess the effect of adaptive convergence on phylogenetic divergence, and determine the circumstances in which associated homoplasy is likely to confound phylogeny reconstruction.

---

\* Address for correspondence: pdpolly@indiana.edu

### 9.1.1 Adaptive Zones, Function, and Phylogeny

Adaptive zones are arguably the key to interpreting the relationship of form, function, and phylogeny. Simpson (1944, 1953) introduced the concept of adaptive zones for environmental spaces that accommodate several evolving lineages. Species inside a zone have latitude for phenotypic evolution and speciation, but those that evolve too near the zone's margins are normally weeded out by selection. Simpson hypothesized that new zones are colonized when rapid bursts of 'quantum' evolution propel a species across the selectively disadvantageous space between zones. Any lineage that escapes one zone for another will do so by evolving a new phenotype compatible with its new environment; those that do not escape will remain constrained within the zone's range of phenotypes. The adaptive zone underpinned Simpson's (1945) taxonomic concept of a phenotypically coherent, paraphyletic group, and rejection of that concept by cladists in the 1970s conflated adaptive zones and plesiomorphic characters (Rosen, 1974). During the same period, quantitative geneticists developed sophisticated mathematical models of adaptive peaks, adaptive landscapes, and trait covariances that are conceptually related to adaptive zones, but whose focus was not taxonomic (Lande, 1976, 1986; Kirkpatrick, 1982; Wake et al., 1983; Wright, 1988; Cheverud, 1996; Schluter, 1996; MacLeod, 2002; Polly, 2004, 2005; Salazar-Ciudad and Jernvall, 2004; Zelditch et al., 2004). Arnold et al. (2001) summarized much of the latter literature. In this paper, I will explore adaptive zones from the conceptual advantage of the quantitative genetics models, but apply them to problems of phylogeny.

For the purposes of this study, I operationally redefine adaptive zone as a bounded range of phenotypes that can be linked to a recognizable functional roles. Phenotypes are emphasized because they can be measured more objectively than the seemingly endless number of potentially constraining environmental variables like the ones suggested by Simpson (1944, 1953); testing selected a set of phenotypes for association with specific environmental variables is more feasible than testing a block of environmental variables for association with all phenotypes. Adaptive zone boundaries are recognized not as gaps in phenotype distribution – these, too, are difficult to objectively measure – but as margins of phenotypic space that are not normally crossed by phylogenetic trajectories and outside which the phenotype is incompatible with the range of functional parameters associated with the zone. Those lineages which do cross the boundaries must do so in association with changes in both their functional ecology and their phenotype if the zone is to be considered an adaptive one. Within the zone boundaries, we can expect that, given enough phylogenetic time, clades will have crisscrossed the phenotypic space as they converged on the finite number of functionally compatible morphologies. Thus, to recognize an adaptive zone using this operational definition: (1) the

zone must be occupied, (2) the zone's occupants must have diversified throughout the zone, and (3) the phylogeny of the occupants must be at least partly known. Unoccupied or recently occupied zones may exist, but they cannot be unambiguously identified from the viewpoint adopted here.

The implication for phylogeny reconstruction is that long term occupation of an adaptive zone will increase the likelihood of convergent evolution, with phenotypic reticulation within the zone obscuring the recoverable phylogenetic history. Clades that escape from the adaptive zone will be difficult to associate with their closest relatives within it. Phylogenetic reconstruction will not be adversely affected if a clade is not evolving within the confines of an adaptive zone or if the zone is recently occupied and has not been fully explored. In those cases, phenotypic convergence will be no more common than expected by chance and phylogeny will be recoverable.

### 9.1.2 Fissipeds and Pinnipeds

Adaptive zones and phylogeny are explored in the Carnivora. This placental mammal order is diverse today, has a plentiful, well-studied fossil record, has a well-understood phylogeny, has evolved many locomotor types, and has been subject to numerous locomotor functional studies. Living carnivorans are divided phylogenetically into two major clades, Feliformia (or Aeluroidea), containing felids, hyaenids, viverrids, and herpestids, and Caniformia, containing canids (Cynoidea), ursids, mustelids, and procyonids (Arctoidea), and pinnipeds. Functionally, Pinnipedia (seals, sea lions, and walruses) are often distinguished from their more terrestrial kin, known collectively as Fissipedia. Some classification schemes, including Simpson's (1945), awarded pinnipeds a coordinate taxonomic rank to other carnivorans, even though the close relationship of pinnipeds to arctoid caniforms has never been seriously questioned.

Pinnipeds are specialized in many ways for their marine lifestyle (Howell, 1930; Bininda-Emonds and Gittleman, 2000), but most important for this paper is their derived locomotor morphology (Figure 9.1). Pinnipeds use their limbs for propulsion in the water – sea lions (Otariidae) use their fore limbs, seals (Phocidae) their hind limbs, and walruses (Odobenidae) both. The digits of both limbs are modified from the terrestrial condition into long flippers that trail fully extended behind the body while swimming. Sea lions and walruses are capable of dorsiflexing the hind foot into a plantigrade position, but seals are prevented from doing so by modifications of the tarsals and the attached tendons and ligaments (Howell, 1929, 1930). The proximal tarsal bones – calcaneum and astragalus – of pinnipeds thus differ in form and function from those of fissiped mammals. A further aim is to compare pinniped and fissiped tarsals in their functional and phylogenetic context, assessing evidence for a fissiped adaptive zone and a higher rate of tarsal evolution in the lineage leading to pinnipeds.

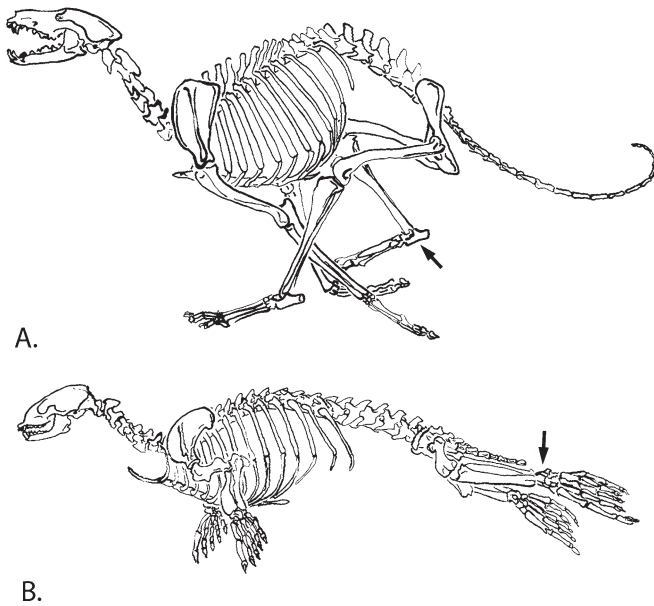


FIGURE 9.1. Skeleton of *Canis familiaris*, the domestic dog (A) and *Phoca vitulina*, the Harbour seal (B). (After Gregory, 1951.) Arrows point to the calcaneum and astragalus.

The diverse morphologies of living carnivorans are the result of approximately 40 million years of evolution. The earliest members of Carnivora, the viverravids, are older than that, coming from the late Paleocene of North America (Fox and Youzwyshyn, 1994; Polly, 1997); however, it is likely that these animals lie outside the crown group (Gingerich and Winkler, 1985; Wesley-Hunt and Flynn, 2005) making the age of the last common ancestor of the living species about 40 Ma (Megannum, or million years ago; Flynn, 1996).

### 9.1.3 Szalayian Analysis

The issues explored in this paper are not new. In paleontology, Szalay especially has written on the role of function in phylogeny reconstruction (Szalay, 1977a,b, 1981, 1994, 2000; Szalay and Bock, 1991; Szalay and Schrenk, 1998; Salton and Szalay, 2004). Building on the work of Bock (1965; Bock and Von Wahlert, 1965), Szalay advocated that functional analysis is required for assessing phylogenetic transformations. All phylogenetic hypotheses are, explicitly or implicitly, statements about character transformation. One of Szalay's points was that transitions in multiple characters must be functionally compatible with one another. Phylogenetic algorithms that treat characters as independent may produce biologically impossible transitions if functional integration was not considered at the stage of character definition. The use of character complexes and the rejection of automated tree optimization algorithms are major planks of the Szalay platform. For Szalay, the character complex is a rich, multidimensional source of phylogenetic data whose states can be compared among taxa, whose transformations can be tested for functional compatibility, and whose form has

biological meaning, especially for reconstructing the lifestyles of incompletely preserved fossil taxa. The masticatory system, especially occluding cheek teeth, and the limbs, particularly interlocking tarsal bones, are conducive to Szalayian analysis because of their physical integration, their direct relevance to an animal's lifestyle, and their common preservation as fossils. An additional goal of this paper is to quantify the Szalayian analysis of tarsal evolution using geometric morphometrics. These techniques are ideal for quantitatively representing three-dimensional morphology, assessing correlations, testing associations with extrinsic functional and ecological data, and building trees (Rohlf and Slice, 1990; Bookstein, 1991; MacLeod and Rose, 1993; Dryden and Mardia, 1998; MacLeod, 1999; Rohlf and Corti, 2000; Polly, 2003a,b). Specifically, I will analyze the major patterns of covariation within the carnivore calcaneostragalus complex to extract components associated with locomotor types, stance, number of digits, body mass, and the covariation of occluding surfaces of the two bones. I will explore the structural transformations of the complex in the context of current understanding of the phylogeny to assess the conditions under which quantitative phylogenetic reconstruction will be accurate.

For this paper, I developed a method for the three-dimensional geometric analysis of bone surfaces. As currently practiced, geometric morphometrics is limited to using a few landmark points or outline curves to represent a complex morphological structure, but functional bone characters are best studied as parts of complete three-dimensional structures. The technique used here is fundamentally the same as the geometric analysis of landmarks and outlines, but it uses as its data the complete surface of an object rather than the limited representation derived from points or curves. An advantage of this approach is that joint surfaces and bony processes are fully incorporated in the analysis and depicted in the results, making it possible to assess the quantitative results of statistical manipulations with the same visual criteria that would be used for a physical bone. A second advantage, and perhaps the more important one, is that the analysis can be applied to any homologous bone, regardless of its derived evolutionary transformations. Standard measurement or landmark morphometrics can only be applied when each bone has precisely the same component structures. If, for example, a bony process is present in only a few taxa, it cannot normally be incorporated into a quantitative analysis of all taxa. By analyzing the complete surface of homologous bones, the presence or absence of individual structures does not impede quantitative analysis so long as the bones can be placed in comparable orientations.

### 9.1.4 Tarsal Morphology and Function

The calcaneum and astragalus (or talus) will be analyzed in this paper (Figure 9.2). These two bones are the largest of the tarsals, or ankle bones, and lie distal to the tibia and fibula and proximal to the rest of the foot. The upper ankle joint (UAJ) lies proximal to them, formed by the large,

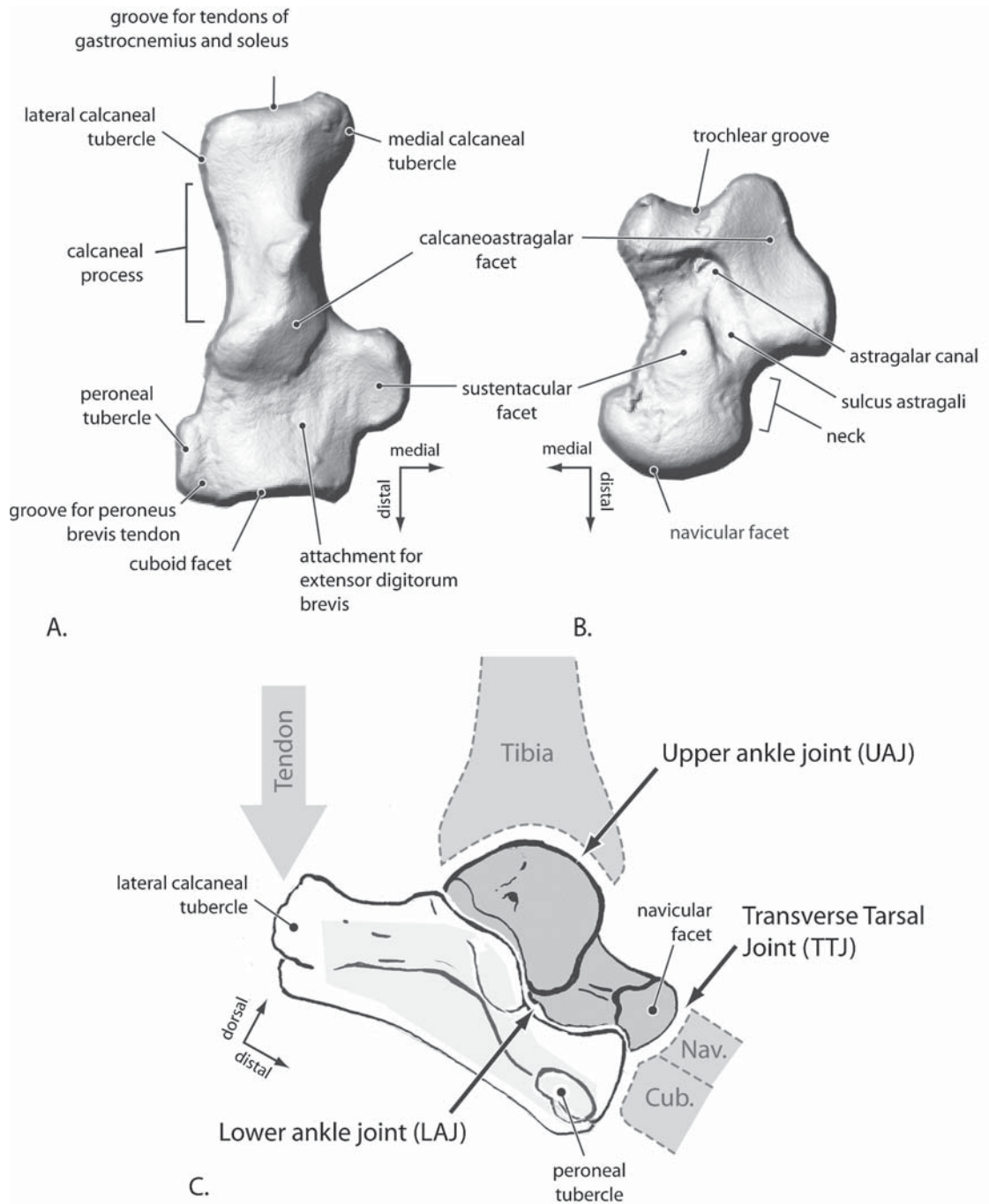


FIGURE 9.2. Morphology of the right calcaneum (A, dorsal view) and astragalus (B, plantar view) of the Badger, *Meles meles*. The bones fit together by flipping the astragalus over to the left so that its calcaneoastagalar and sustentacular facets occlude against those with the same name on the calcaneum (C). The sustentacular and calcaneoastagalar facets of the two bones are the primary contact surfaces of the lower ankle joint.

dorsal trochlea of the astragalus and the concave, contoured surface on the distal ends of the tibia and fibula. In carnivores, movement at this joint is associated with dorsiflexion and plantarflexion of the foot. Plantarflexion, an important propulsive movement on land or in water, is powered by the large gastrocnemius and soleus muscles, which insert at

the proximal end of the calcaneal process. The astragalar trochlea forms the fulcrum of the joint, and the calcaneal process the moment arm of effort. The lower ankle joint (LAJ) lies between the astragalus and calcaneum and moves along two pairs of occluding facets. The calcaneoastagalar facets lie on the medial margin of the ventral side of the astragalus

body and the medial side of the dorsal calcaneum. These are usually long and proximodistally oriented on both bones, with the astragalar facet concave and the calcaneal one convex. The sustentacular facets lie on the ventral side of the astragalus neck and on the dorsal side of the sustentacular process on the medial side of the distal calcaneum. These are usually subcircular in outline, with the astragalar facet convex and the calcaneal facet concave. Movement at the LAJ varies considerable among carnivorans. In terrestrial digitigrade taxa the LAJ may be tightly interlocked, allowing only small movements, but in arboreal taxa considerable movement at the LAJ may be associated with foot inversion. The transverse tarsal joint (TTJ) lies between the astragalus head and distal calcaneum on the one hand, and the proximal faces of the navicular and cuboid bones on the other. Movement at the TTJ also varies in Carnivora, but includes foot inversion and eversion. Other functionally important features of the tarsals include the medial and lateral calcaneal tubercles, which are sites of origination for flexors of the digits and sites of insertion for the plantarflexors of the ankle. The peroneal tubercle has grooves on the dorsal and plantar sides for the peroneus brevis and longus respectively and functions in flexion and inversion-eversion of the foot. The proportional lengths of the calcaneal process, the distal calcaneum (anterior to the calcaneo-astragalar facet), and the astragalar neck are related to the lever advantages of dorsiflexion and plantarflexion. The breadth of the distal calcaneum, especially as contributed by the peroneal tubercle and sustentacular process, are partly related to lever advantages of foot inversion and eversion. Taylor (1989) reviewed locomotor morphology in Carnivora. Important original studies of carnivoran hind limb functional morphology include Howell (1929), Hildebrand (1954), Taylor (1970, 1976, 1988), Howard (1973), Jenkins and Camazine (1977), Goslow and Van de Graff (1982), Jenkins and McClearn (1984), Van Valkenburgh (1985), and Evans (1993). General references on functional morphology of the hindlimb in mammals include Howell (1944), Clevedon-Brown and Yalden (1973), Gambaryan (1974), Szalay (1977a, 1994), Lewis (1989), and Alexander (2003).

## 9.2 Materials and Methods

### 9.2.1 Materials

Twelve species were chosen to represent carnivoran phylogenetic and locomotor diversity (Table 9.1). All family-level groups except Ursidae were included, with representation balanced across the three major divisions Aeluroidea, Canoidea, and Arctoidea. *Phoca groenlandica*, the Harp seal, represented the pinnipeds. Seals have the most highly derived locomotor morphology of the pinnipeds (King, 1966; Wyss, 1988) and thus maximize differences between the pinniped and fissiped morphologies, giving the best chance to detect a high rate of phenotypic divergence.

Associated data were taken from published literature and personal observations. Average body mass was calculated from data compiled by Silva and Downing (1995), except for *Bassaricyon* (Eisenberg, 1989), and the domestic Greyhound (Kennel Club, 1998). Locomotor types follow Van Valkenburgh (1985) and Taylor (1976, 1989). Terrestrial animals spend most of their time on the ground (e.g., dogs and hyenas); scansorial animals spend considerable time on the ground, but are also good climbers (e.g., most felids); arboreal animals spend most of their time in trees (e.g., olingos, red pandas); natatorial animals spend time in both the water and on land (e.g., otters); and aquatic animals spend most time in water and are only capable of awkward locomotion on land (e.g., seals, sealions). Stance refers to the position of the heel during normal locomotion (Clevedon Brown and Yalden, 1973; Gambaryan, 1974; Gonyea, 1976; Hildebrand, 1980). Plantigrade animals walk with their heels touching the ground (e.g., red pandas); semidigitigrade animals often keep their heels elevated during locomotion (e.g., many mustelids); and digitigrade animals always have their heels elevated during normal locomotion, using the metatarsus as an additional limb segment (e.g., dogs, felids). The combination of stance and locomotor type distinguishes some common categories, such as ambulatory from cursorial. Pinnipeds do not fall into normal stance categories and so have been classified as

TABLE 9.1. Carnivoran species and associated data used in this study.

Species	Common name	Family	Body mass (kg)	Stance	Digits	Locomotor type
<i>Ailurus fulgens</i>	Red panda	Ailuridae	5.1	Plantigrade	5	Arboreal
<i>Bassaricyon gabbii</i>	Bushy-tailed olingo	Procyonidae	1.2	Plantigrade	5	Arboreal
<i>Canis familiaris</i>	Dog (Greyhound)	Canidae	29.0	Digitigrade	4	Terrestrial
<i>Crocuta Crocuta</i>	Spotted hyaena	Hyaenidae	63.9	Digitigrade	4	Terrestrial
<i>Felis catus</i>	Domestic cat	Felidae	3.7	Digitigrade	4	Scansorial
<i>Leptailurus serval</i>	Serval	Felidae	10.6	Digitigrade	4	Terrestrial
<i>Lutra lutra</i>	European otter	Mustelidae	7.4	Semidigitigrade	5	Natatorial
<i>Lynx rufus</i>	Bobcat	Felidae	9.6	Digitigrade	4	Scansorial
<i>Meles meles</i>	Badger	Mustelidae	10.7	Semidigitigrade	5	Semifossorial
<i>Mustela putorius</i>	Polecat	Mustelidae	1.0	Semidigitigrade	5	Terrestrial
<i>Paradoxurus hermaphroditus</i>	Palm civet	Viverridae	3.1	Semidigitigrade	5	Arboreal
<i>Phoca groenlandica</i>	Harp seal	Phocidae	167.0	Specialized	5	Aquatic

“specialized”. Number of toes on the hind foot was recorded as four or five.

### 9.2.2 Scanning and Post-processing

The calcaneum and astragalus of each species were scanned in three dimensions. The calcaneum was scanned in dorsal view. Most of the functional features of the calcaneum are on the dorsal side, including the sustentacular facet, the astragalocalcaneal facet, and many muscle and tendon attachments. The astragalus was scanned in plantar (ventral) view. The plantar surface of the astragalus contains the structures that directly interface with the calcaneum. The dorsal side of the astragalus also contains important functional features, such as the trochlea, which were not analyzed.

Scans were made with a Roland PICZA PIX-4 pin scanner. This instrument records the Cartesian  $x y z$  coordinates of an object's surface by translating it in the  $x$  dimension below a carriage that moves along the  $y$  dimension. The carriage drops a pin to touch the object, recording the  $z$  coordinate. The density of  $x y$  point coordinates can be set between 0.05 and 5 mm; the density of  $z$  depends on the vertical relief of the object, with a higher density recorded on flatter surfaces. Several recent studies used such pin scanners (e.g., Eguchi et al., 2004).

Resolution of the tarsal scans was set according to the size of the bone. The smallest species, *Mustela putorius*, was scanned at 0.05 mm  $x y$  density, which produced a point grid of about  $100 \times 55$  points; large species, such as *Canis familiaris*, were scanned at a lower density of 0.40 mm to produce a similar size point grid. Fine detail, including bone texture, was visible at these resolutions.

The lower  $z$  margins of the scans were standardized because variation in scan depth would influence the apparent variation in shape. Data were standardized by truncating each calcaneum scan just below the level of the sustentacular process

and each astragalus scan just below the neck margin. Because the spacing of points in the  $z$  dimension depends on the slope of the surface, the lower  $z$  margin was irregular. To prevent the irregularity from influencing the shape comparisons, the margin was evened by dropping a series of new points to a  $z$  value of 0.0 directly below the original margin points.

### 9.2.3 Three-dimensional “Fishnet” Surface Points

Each bone was characterized for morphometric analysis with points interpolated across the surface. Quantitative comparisons of shape require that each surface be represented by an equal number of points. Different scan resolutions and bone sizes produce point grids that cannot be compared without interpolating an equal number of regularly spaced points on each surface.

Interpolation was a two step process. First an equal number of points were interpolated on each row of the original scan coordinates from proximal to distal. The original scan coordinates formed an  $n_j \times j$  matrix, where  $n_j$  was the number of points in row  $j$ , and  $j$  was the number of rows along the proximal-distal axis. Each  $n_i$  row was replaced with  $m$  interpolated points to produce an  $m \times j$  matrix of points. The algorithm used for standard eigenshape analysis was used to interpolate each row (Lohmann, 1983; Lohmann and Schweitzer, 1990; MacLeod, 1999; MacLeod and Rose, 1993). Then for each  $m$ , a  $k$  number of evenly spaced points were interpolated to produce an  $m \times k$  matrix of points.

The resulting interpolated surface can be likened to an elastic fishnet stocking stretched around the object (Figure 9.3). Each node of the stocking fabric represents a point on the surface. Before fitting, the nodes are equally spaced, but on the object they are stretched to fit the contours of the surface beneath them.

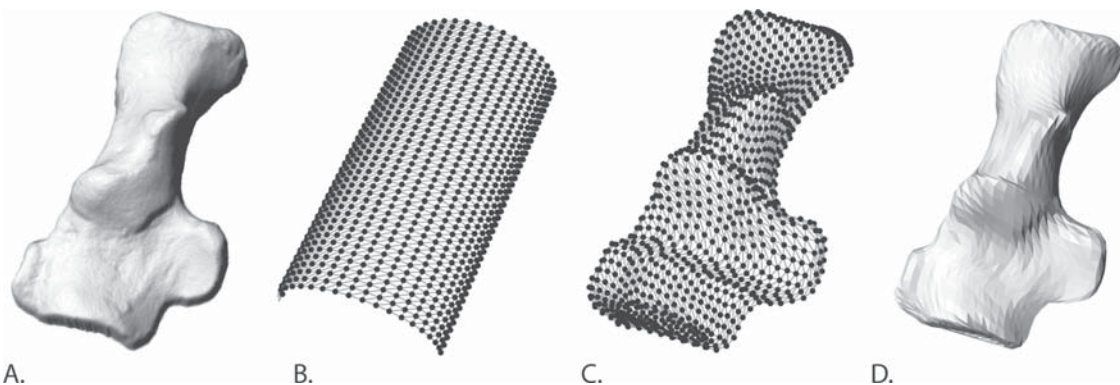


FIGURE 9.3. A, Calcaneum of *Meles meles*, three-dimensional rendering of original scan. B, three-dimensional “fishnet” point grid before fitting. C,  $25 \times 50$  point fishnet grid fit to the calcaneum of *Meles*. D, Raster rendering of the fishnet grid to show quality of resolution. Surface lines are an artefact of the interpoint mesh representation used to make the rendering.

A fishnet grid of  $25 \times 50$  points was placed on each calcaneum, with the first point at the distolateral corner of the bone and the last at the proximomedial corner. A  $25 \times 30$  grid was placed on each astragalus in the same orientation. Because of computational limitations, the number of points was reduced to  $20 \times 50$  and  $20 \times 30$  respectively for two-block partial least squares analysis.

### 9.2.4 Ordination and Shape Modeling

Bone surfaces were aligned to a common size and orientation using Procrustes analysis. Each set of fishnet surfaces was translated, rotated, and rescaled to unit size using the generalized least squares Procrustes algorithm described by Rohlf (1990) and Rohlf and Slice (1990). An orthogonal projection into shape tangent space was applied using the algorithm of Rohlf and Corti (2000). To create a standard orientation for quantitative analysis, the aligned shapes were rotated to their three-dimensional principal components.

The bones were ordinated in shape space using principal components analysis (PCA; Dryden and Mardia, 1998). The consensus, or mean shape, was subtracted from each set of aligned fishnet surfaces. This step centers the shape space on the mean shape. A covariance matrix was calculated from the resulting residuals. PC vectors were calculated from the singular value decomposition of the covariance matrix:

$$\text{SVD}[\mathbf{P}] = \mathbf{U}\mathbf{S}\mathbf{V}^T \quad (9.1)$$

where  $\mathbf{P}$  is the covariance matrix of the Procrustes residuals,  $\mathbf{U}$  is the matrix of PC vector weightings,  $\mathbf{S}$  is the matrix of singular values, and  $\mathbf{V}$  is the transpose of  $\mathbf{U}$  (when  $\mathbf{P}$  is square, symmetric, positive definite covariance matrix).

The computationally limiting factor for three-dimensional surface analysis was the size of the covariance matrix. Matrices for three-dimensional surfaces are large because of the number are the number rows in each direction of the fishnet and 3 is the number of dimensions of each point. For the  $25 \times 50$  calcaneum fishnet, the covariance matrix had 14,062,500 cells, requiring more than 112Mb of memory. The efficiency of the analysis can be improved by doing the SVD on the covariance matrix of the objects rather than variables. In this case, the 12 taxa require a very small matrix of  $12 \times 12$ , or 144 cells. The eigenvectors and eigenvalues for the variable matrix can be back-calculated from those of the object matrix.

The coordinates of each bone in the PC shape space are called scores. The scores were used as shape variables for statistical analysis and tree building. Each bone has a score on every PC axis. The consensus shape has a score of 0.0 on each axis because it lies at the center of the shape space. Scores were calculated as  $\mathbf{R}\mathbf{U}^T$ , where  $\mathbf{R}$  is the matrix of surface residuals and  $\mathbf{U}^T$  is the transpose of  $\mathbf{U}$ .

Every point in the PC shape space corresponds to a different three-dimensional surface, regardless of whether a real bone lies there or not. Shapes at any particular point can be

modeled by multiplying the value of the position on the PC axis by the corresponding vectors and adding the shape consensus to the result. Modeling can be done in the full multi-dimensional space or at positions along particular vectors or subsets of vectors. The former is useful for representing the shape of a particular taxon or locomotor category, whereas the latter is useful for illustrating the range of shapes associated with a particular PC or PLS axis. The estimated shape is:

$$\hat{X} = \mathbf{P}\mathbf{U}^T \quad (9.2)$$

where  $\hat{X}$  is the modeled shape,  $\mathbf{P}$  is the position being modeled, and  $\mathbf{U}^T$  is the transpose of the vectors being modeled.  $\hat{X}$  is a vector of three-dimensional fishnet points. These can be represented as points with or without a connecting mesh (Figure 9.3c) or as a shadowed surface rendering of the surface defined by the points (Figure 9.3d). The shadowed renderings in Figures 9.3, 9.7–9.9, 9.11, 9.12, and 9.16 were created by importing  $\hat{X}$  into Rhinoceros 3.0, a three-dimensional vector graphics program.

### 9.2.5 Facet Size and Shape

The size and shape of joint facets were analyzed using the original scan data. The sustentacular and calcaneoastragalus facet surfaces were extracted from both the calcaneum and astragalus of each taxon (Figure 9.4a) and the margin of each synovial capsule was traced. Facet area was calculated in  $\text{mm}^2$ .

Facet curvature was measured as the curvature of a sphere fit to the surface of the facet. To do this, the surface area was first converted to  $x y z$  coordinates (Figure 9.4b) and rotated to its principal components with the concave side up. The rotation provided a common, horizontal orientation for comparison. The center of the facet was estimated by calculating the centroid (or arithmetic average) of the surface coordinates. The centroid of a three-dimensional shape, such as these facets, does not necessarily lie on the surface itself, so the center of the facet was estimated as the projection of the centroid onto the surface along the  $z$  axis. The rate of curvature was represented as the coefficient of curvature of a sphere fit to the surface and passing through the center point. The fit was achieved by subtracting the coordinates of the center point from the surface points and fitting the function  $\hat{Z} = bx^2$  (Figure 9.4c). The coefficient  $b$  was used as the measure of curvature. For perfectly flat facets, height on the  $z$  axis does not increase away from the center and  $b = 0$ ; for curved facets, height on the  $z$  axis increases away from the center and  $b > 0$ . Because the facets were compared concave side up regardless of whether the surface on the bone was concave or convex, all coefficients of curvature were positive.

The fit of occluding facets was measured as the ratio of the larger or most curved of the occluding facets over the smaller or less curved. The index of fit for area was:

$$\text{Index}_{\text{area}} = \frac{\text{area}_{\text{max}}}{\text{area}_{\text{min}}}, \quad (9.3)$$

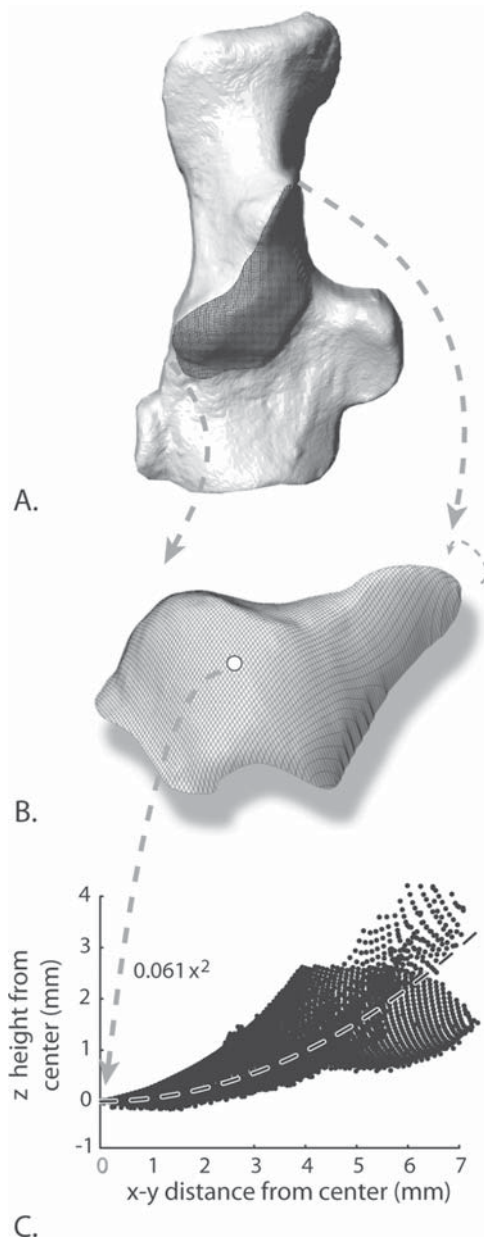


FIGURE 9.4. The measurement of facet curvature. A, The boundaries of the synovial capsule are traced on the surface of the bone. B, The facet is extracted and its centroid found (white circle). C, Each surface point is plotted by its  $x$   $y$  distance and  $z$  height from the centroid when the facet is in a standard orientation. Curvature is measured by fitting the equation  $y = ax^2$  to these transformed data. The coefficient  $a$  is larger when the surface is more curved.

where  $area_{max}$  is the larger of the two occluding facets and  $area_{min}$  is the smaller. The index for curvature was the same as Equation 9.3, but with  $b$  substituted for  $area$ . The index equals 1 when the occluding facets are the same size (or curvature) and increases with increasing discrepancy in size (or curvature). No data on errors estimating the area or curvature of the facets are available, but differences less than 0.3 are unlikely to be significant.

### 9.2.6 Two-block Partial Least Squares

The evolution of a form-function complex, such as the occluding faces of the astragalus and calcaneum, is an integrated process (Bock and von Wahlert, 1965; Szalay and Bock, 1991; Szalay, 2000). In order for the form of one bone to change, the form of the other must change in a compatible fashion, especially those parts that contact one another. One method for extracting correlated variation in the astragalus and calcaneum is two-block partial least squares analysis (2B-PLS). 2B-PLS extracts correlated shape variation as a series of orthogonal vector pairs (Sampson et al., 1989; Rohlf and Corti, 2000). In this study, each vector pair describes correlated variation in the plantar astragalus and dorsal calcaneum respectively. Different pairs are mathematically independent of one another such that change along one vector could, in principle, occur independently of that on another while still maintaining functional integration between the shapes of the two bones. Pairs of 2B-PLS vectors are ordered by the proportion of covariation they explain, with PLS 1 explaining the largest portion.

2B-PLS was performed on the matrix of covariances of the astragalus and calcaneum surface coordinate. Because of computational limitations mentioned above, smaller fishnet grids were used to represent each bone than for other analyses. Each bone was Procrustes superimposed, rotated to its principal components, and projected into orthogonal tangent space. Procrustes residuals were calculated by subtracting the consensus configuration. The matrix of covariances between astragalus and calcaneum residuals was calculated. 2B-PLS vectors and singular values were calculated by SVD of the covariance matrix following Rohlf and Corti (2000). 2B-PLS scores were calculated by projecting the shapes onto the vectors as described above. Shape variation on the 2B-PLS axes was modeled as described above.

### 9.2.7 Maximum-likelihood Trees

Tree diagrams are useful for depicting the similarities between morphometric shapes. Trees can be compared to phylogenies based on independent evidence, to locomotor categories, and to other biological groupings to explore possible causes of shape similarity. Many tree algorithms are available, but one of the most appropriate is maximum-likelihood (ML) method for quantitative traits because it does not assume equal rates of change and it treats independent aspects of shape as separate characters (Felsenstein, 1973, 1981, 1988; Polly, 2003a, b; Caumul and Polly, 2005). The Brownian motion model of evolution used in most ML algorithms appears to be appropriate for multivariate morphological shape (Polly, 2004; see discussion below).

PCA scores were used as the data for tree building. The scores satisfy the requirements for ML because they are uncorrelated and continuously distributed. Scores were standardized to a mean of zero and variance equal to the proportion explained by the corresponding vector. Standardization to unit variance,

which is the usual procedure (Felsenstein, 1973) puts undesirable weight on less important vectors that contain little information about shape. The CONTML module of PHYLIP (Felsenstein, 1993) was used for tree building. Input order of the taxa was randomized and three global rearrangements were made.

### 9.2.8 Reconstruction of Ancestral Morphologies

Morphological shape scores can be reconstructed at the nodes of a phylogenetic tree when branch lengths and the shape of all terminal taxa are known using any one of the several available methods (Grafen, 1989; McARDLE and RODRIGO, 1994; MARTINS and HANSEN, 1997; GARLAND et al., 1999; GARLAND and IVES, 2000; POLLY, 2001; ROHLF, 2001). The estimated ancestral shape can be modeled from the reconstructed scores using the modeling procedure described above. Importantly, the phylogenetic tree can be projected into the morphospace by projecting the node scores into the space and connecting the branches. Such a projection provides a visual means of assessing the history of phylogenetic occupation of the morphospace.

The generalized linear model (GLM) method of estimating ancestral states (Martins and Hansen, 1997) was used here to reconstruct node scores. This method requires two matrices derived from the phylogenetic tree. The phylogenetic error variance matrix,  $\text{var}[\mathbf{Y}]$ , is an  $n \times n$  matrix, where  $n$  is the number of terminal taxa. The diagonal contains the length from the taxon to the base of the tree and the off diagonal elements contain the length from the last common ancestor of two taxa to the bottom of the tree. The node error variance matrix,  $\text{var}[\mathbf{A}, \mathbf{Y}]$ , is an  $n \times m$  matrix, where  $n$  is the number of terminal taxa and  $m$  is the number of nodes in the tree. Each element contains the length of shared history between the node and each terminal taxon. The scores at the base of the tree were estimated as:

$$\mathbf{M}_G = (\mathbf{J}' \text{var}[\mathbf{Y}]^{-1} \mathbf{J})^{-1} \mathbf{J}' \text{var}[\mathbf{Y}]^{-1} \mathbf{Y}, \quad (9.4)$$

where  $\mathbf{M}_G$  is the estimated score values at the base of the tree,  $\mathbf{J}$  is a unit vector of length  $n$ , and  $\mathbf{Y}$  is the matrix of scores of the terminal taxa. The other node values are then calculated from the residuals of the scores from the node reconstruction as:

$$\hat{\mathbf{A}} = \text{var}[\mathbf{A}, \mathbf{Y}] \text{var}[\mathbf{Y}]^{-1} \mathbf{Y}' + \mathbf{M}_G, \quad (9.5)$$

where  $\hat{\mathbf{A}}$  are the estimated node scores and  $\mathbf{Y}'$  is the matrix of residual scores after the subtraction of  $\mathbf{M}_G$ .

Ancestral shapes were reconstructed on a phylogenetic tree derived from Flynn (1996). Some points about carnivoran phylogeny are controversial. The broad agreement 15 years ago on relationships among the major family-level groups (e.g., Flynn et al., 1988; Wayne et al., 1989; Wozencraft, 1989; Wyss and Flynn, 1993; Wolsan, 1993, but see Hunt and Tedford, 1993) has dissolved with subsequent studies (Lento et al., 1995; Slattery and O'Brien, 1995; Ledge and Arnason, 1996a, b; Flynn, 1996; Werdelin, 1996;

Wang, 1997; Flynn and Nedbal, 1998; Janis et al., 1998; Koepfli and Wayne, 1998, 2003; Flynn et al., 2000; Veron and Heard, 2000; Gaubert and Veron, 2003; Sato et al., 2003; Sato et al., 2004; Davis et al., 2004; Veron et al., 2004; Yu et al., 2004; Flynn and Wesley-Hunt, 2005; Flynn et al., 2005; Wesley-Hunt and Flynn, 2005; Yu and Zhang, 2005). Only the dichotomy between Feliformia and Caniformia remains completely uncontroversial, at least with respect to the taxa included here. I did not use the consensus "super-tree" of Carnivora (Bininda-Emonds et al., 1999) because of the well-known pitfalls affecting consensus trees that are based on different, overlapping datasets (Miyamoto, 1985; Kluge, 1989).

The tree adopted for ancestral reconstruction is shown in Figure 9.5. The choice of this tree did not affect ancestral node reconstructions because the controversial nodes, such as the phylogenetic placement of the Red panda, *Ailurus*, are closely spaced in geological time. The three feliform groups – Hyaenidae, Viverridae, and Felidae – diverged around 22Ma, regardless of which of the three are most closely related. The shared history of the two most closely related was brief relative to the history shared by all three. The duration of shared history exerts more influence on ancestral reconstruction than the ordering of closely spaced branching events (Martins and Hansen, 1997; Polly, 2001). Reversing the order of branching among *Paradoxurus*, *Crocota*, and the felids would not change the reconstruction at those nodes (because of that, I have grouped the nodes together as Node 1). Similarly, Canidae, Phocidae (and other pinnipeds), *Ailurus*, Procyonidae, and Mustelidae shared a last common ancestor around 36Ma. The lineages leading to the three mustelids – *Lutra*, *Mustela*, and *Meles* – branched in quick succession around 24Ma, and these have been grouped as Node 4 for purposes of ancestral reconstruction. The divergence times are the younger of Flynn's (1996) two estimates, which are the ones supported by recent palaeontological studies (Wesley-Hunt and Flynn, 2005).

Ancestral node reconstructions have large confidence intervals (Martins and Hansen, 1997; Garland and Ives, 2000; Polly, 2001). The reconstructed shapes are those that are the most likely given the morphology of the terminal taxa and the topology of the tree; however, many other shapes are both biologically and statistically plausible. The range of statistically likely shapes can be described by a 95% confidence spheroid in shape space with the optimal reconstruction at its centre. At the deep nodes of the tree, these spheroids will encompass the range of variation found in the terminal taxa, something that should be remembered when comparing the reconstructions to real fossil taxa. No attempt was made to model the range of shapes falling within the node confidence spheroids, though it is easily done (Martins and Hansen, 1997), because a very large number of reconstructions would be required to give even a hint of the morphological range encompassed by a confidence spheroid in the 11-dimensional shape space.

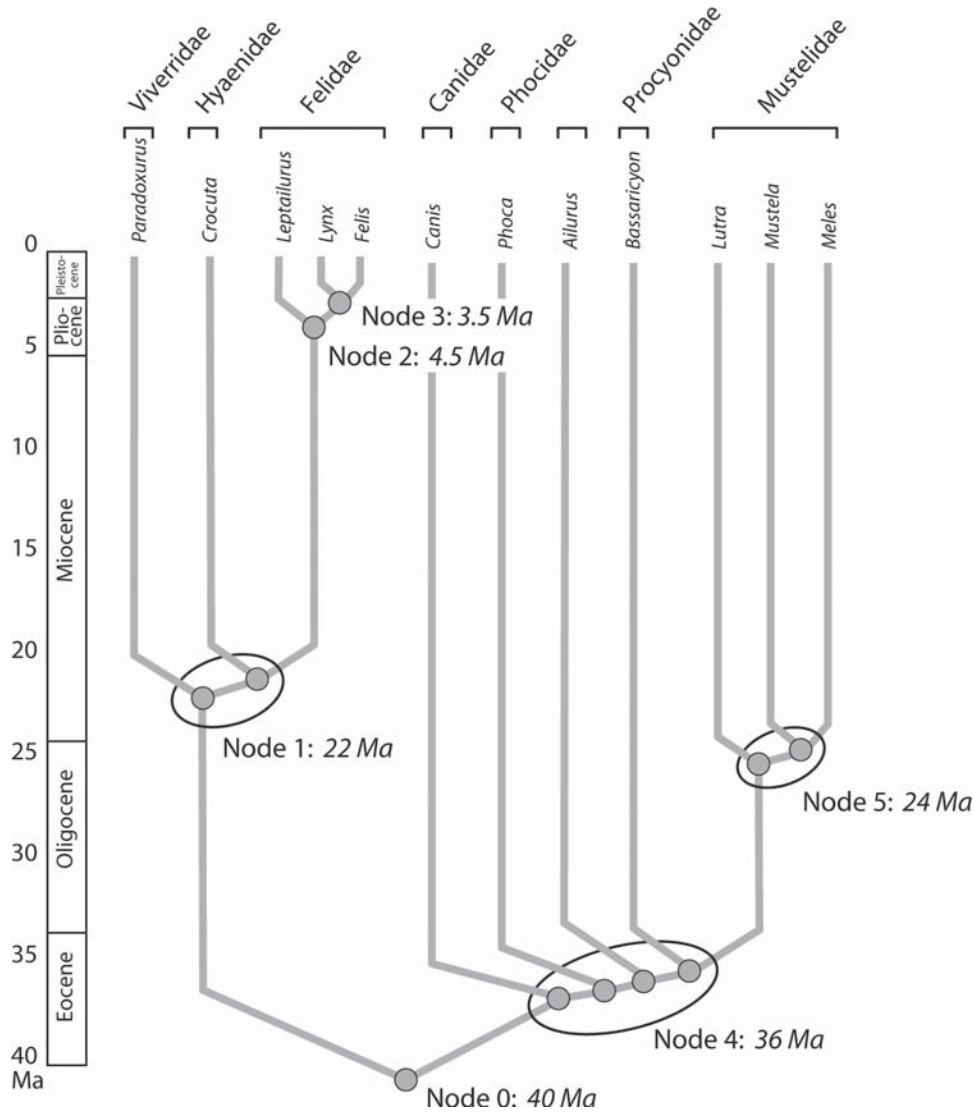


FIGURE 9.5. Phylogenetic tree of the twelve carnivorous species. The topology and branch lengths are based on Flynn (1996). Nodes whose estimated divergence times are equal were combined for purposes of ancestral shape reconstruction.

### 9.2.9 Rates And Mode of Tarsal Evolution

Rate of morphological evolution was quantified as Procrustes distance over time. Procrustes distance is the sum of distances between corresponding fishnet points when two bones are in optimal superimposition:

$$D = \sqrt{\sum_{i=1}^{m \times k} (p_{1i} - p_{2i})^2} \tag{9.6}$$

where  $p_{1i}$  and  $p_{2i}$  are points  $i$  on bones 1 and 2, and  $m \times k$  is the total number of points.

Rates along individual tree branches were calculated by dividing the squared distance between the end shapes by the length of the branch. Shapes at terminal branches are the interpolated point grids from the original scans and the shapes

at the nodes are the ancestral reconstructions. Squared distances were used because morphological variance increases linearly with time when there is a Brownian motion mode of evolution (Felsenstein, 1988; Polly, 2004), making  $D^2$  rates less biased than ordinary ones. Rate estimation depends on the accuracy of node reconstructions. The optimal reconstructions used here minimize rates across the tree. Alternative reconstructions increase some branch rates at the expense of others, but also increase the average rate across all branches. For tree-specific rates, branch length was measured in generations, which are the natural units of evolutionary processes (Gingerich, 1993, 2001; Polly, 2001, 2002). Lengths were converted from millions of years to generations using a mean carnivorous generation length – 3.8 years – calculated from data compiled by Eisenberg (1981).

The pattern of shape divergence over time was used to estimate the mode of evolution. By mode, I mean the pattern of divergence resulting from long-term directional, stabilizing, or randomly varying selection (Polly, 2004). Long-term directional selection continually pushes all species in the same direction, causing correlated evolution among lineages. An example would be the general increase in size expected under Cope's Rule (Stanley, 1973; Alroy, 1998; Polly, 1998; Van Valkenburgh et al., 2004). Stabilizing selection prevents species from evolving away from some optimum, and is variously called stabilizing selection (Schmalhausen, 1949), centripetal selection (Simpson, 1953), adaptive peak model (Lande, 1976; Felsenstein, 1988), and Ornstein-Uhlenbeck process (Felsenstein, 1988; Martins and Hansen, 1997). Stasis – the complete absence of evolutionary change – is an extreme example. Randomly fluctuating selection changes direction and magnitude, usually as species adapt to new and changing environments. This is a typical Brownian motion process (Lande, 1986; Felsenstein, 1988; Martins and Hansen, 1997) and may include components of directional or stabilizing selection at particular times. The evolutionary pattern produced by randomly fluctuating selection is identical to that produced by neutral genetic drift except in the rate of divergence. Drift is slower and its rate is a function of population size. I subsume drift under randomly fluctuating selection because the data required to distinguish them are unavailable. Evolutionary modes may be distinguished by the scaling relationship of shape divergence to time since common ancestry (Bookstein et al., 1978; Gingerich, 1993; Polly, 2004; Pie and Weitz, 2005). Directional selection causes a constantly increasing, linear divergence. Randomly fluctuating selection causes both divergence and convergence such that shape diverges on average with the square root of time. Stabilizing selection limits divergence so there is no relation with time since common ancestry after a point. That point depends on the strength of the stabilizing selection, the rate of evolution, and the maximum time of common ancestry of the clade.

Mode was estimated by fitting the equation:

$$y = x^a \quad (9.7)$$

where  $y$  is shape difference between two taxa,  $x$  is the time elapsed since their last common ancestor, and  $a$  is a coefficient ranging from 1 to 0. A coefficient of 1 corresponds to directional selection where divergence increases linearly with time. A coefficient of 0.5 corresponds to random selection where divergence increases with the square root of time. A coefficient of 0 corresponds to stabilizing selection where divergence does not increase with time. Intermediate values of  $a$  correspond to random selection with a predominance of stabilizing or directional selection. To find  $a$ , Equation 9.6 was fit to the data using values ranging from 0.1 to 1 at 0.1 intervals. The value that minimized the residual variance was chosen (Butler and King, 2004).

Two measures of time since common ancestry were used. Palaeontological estimates of the age of the last common ancestor of each species pair were taken from the tree in

Figure 9.5 (see above). Cytochrome  $b$  sequence distance was used as a proxy measure (Brown et al., 1979; Springer, 1997). The advantage of  $cyt\ b$  is that it is measured in each species independently, so an error (including atypical mutational history) in one species does not affect all of the pairs. Error in a palaeontological node age affects all species connected through that node. The disadvantage of  $cyt\ b$  is that it is only a proxy for time since common ancestry and has its own set of errors (Graur and Martin, 2004). One such error is saturation, or the effect of “multiple hits”, which causes divergences older than 15–20 million years to be underestimated (Nei, 1987).  $Cyt\ b$  divergence was measured as the Kimura 2-parameter sequence distance, which weights transition and transversion mutations differently and which is corrected for the effects of saturation (Kimura, 1980). Eleven sequences were taken from GenBank.  $Cyt\ b$  was not available for *Leptailurus*. Clustal X, version 1.8 (Thompson et al., 1997) was used to align the sequences and calculate distances.

### 9.2.10 Adaptive Landscape Contours

The fissiped adaptive landscape contours in Figure 9.16 were calculated from the fissiped scores on the first two PCs. Ellipses were centered on the mean fissiped shape and encompass 5 and 95 percentiles. The outer ellipse is equivalent to a 95% confidence interval. In more than two dimensions, the adaptive landscape is a multidimensional spheroid; the ellipses shown in Figure 9.16 are the projection of that spheroid onto the first two PCs.

### 9.2.11 Association of Tarsal Shape and Locomotor Factors

Association of tarsal shape with locomotor mode, stance, toe number, body mass, and the facet indices was tested using regression and one-way analysis of variance (ANOVA). Multivariate analysis of variance (MANOVA) was used to test the entire three-dimensional shape against categorical factors; univariate ANOVA was used to test individual PCs. Significance was determined with a multivariate F, or Wilks' Lambda test.

## 9.3 Results and Discussion

### 9.3.1 The Bones

Twenty-four bones were scanned, two each from the twelve species (Figure 9.6). The most obvious variation in the calcaneum was in the size of the peroneal tubercle, which was largest in *Ailurus* and *Lutra* and nearly absent in *Crocota* and *Phoca*. The position and size of the sustentacular process also varied from a proximal position in the three felids to a distal position in *Paradoxurus* and *Bassaricyon*. The shape of the calcaneostragalar facet was proximodistally short and curved in the felids, *Crocota*, and *Canis*, but long and less curved

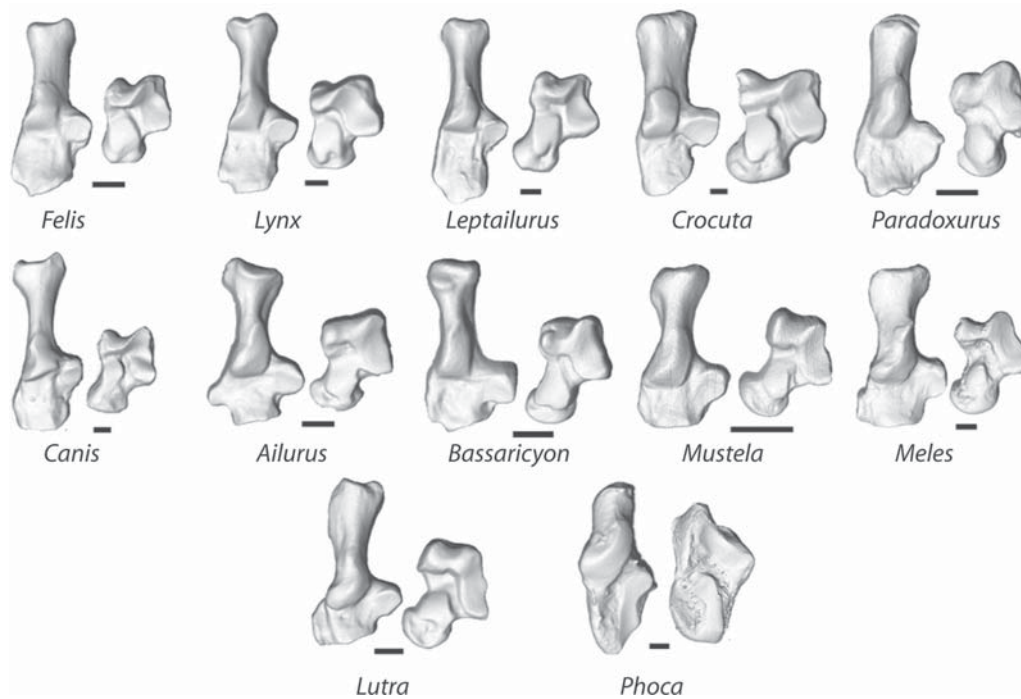


FIGURE 9.6. Three-dimensional scans of the right calcaneum (dorsal view) and astragalus (plantar view) from 12 carnivorans. Orientations are the same as in Figure 9.2. Scale bars equal 5 mm.

in other taxa. The length of the calcaneal tubercle was proportionally long in *Lutra*, but shorter in the felids. The bony processes of the tubercle also varied, especially in their degree of lateral and medial asymmetry. On the astragalus, the length of the neck, the curvature of the calcaneoastragalus facet, and the shape of the body were the most visibly variable features.

The tarsals of *Phoca* were notably different from the fissiped taxa. *Phoca's* calcaneum was diamond-shaped with a pointed distal end. The calcaneal process was short and without lateral tubercles for attachment of the superficial digital flexor. The groove at the end of the calcaneal process for the attachment of the semitendinosus and gastrocnemius was absent. In seals, these tendons probably insert parallel to the long shaft of the bone instead of at a vertical angle (Howell, 1929). The astragalus was blocky without noticeable neck or trochlear groove. A bony process extended from the proximal end of the astragalus, paralleling the calcaneal tuber. This bony process and the tendon for the flexor hallucis longus, which passes along a groove on the process, prevent the foot from being brought into a plantigrade position (Howell, 1929). The calcaneoastragalus and sustentacular facets were long, especially the latter (King, 1966; Wyss, 1998). In fissipeds, the sustentacular facet is always an ovate basin.

### 9.3.2 Principal Component Analysis

Principal component analysis (PCA) was used to construct a phenotypic morphospace for the bones and to extract major

axes of correlation. The results of the PCAs for calcaneum and astragalus are shown in Figures 9.7 and 9.8. Plots of the bones in the first three PC dimensions are shown in the top panels. Each taxon is represented by a shape model calculated from scores on the first three axes. Models of shape variation along the individual PC axes are shown at the bottom of the figures. Each axis is illustrated by five models showing shape variation along the axis at quartile points. The right and leftmost models represent the shape at the positive and negative extremes of variation, and the middle model represents the average, or consensus shape. The consensus models of the three PCs are identical because all axes are centered on the same mean sample shape. Differences among models along a particular PC represent correlated variation, but differences between series represent independent variation. The eigenvalues and percent variance explained by each PC are reported at right.

The shape models in Figures 9.7a and 9.8a represent real bones reconstructed from scores on the first three PCs, but the quartile series in Figures 9.7b–d and 9.8b–d are hypothetical bones constructed from only one PC each. The shape of the *Phoca* calcaneum illustrates this. In Figure 9.7a, the *Phoca* model can be understood as the visual summation of the models in Figure 9.7b–d that correspond to *Phoca's* position on each respective axis. The *Phoca* model can be mentally reconstructed from the PC shape models by combining those at position 0.075 on PC 1, position –0.12 on PC 2, and position 0.09 on PC 3. Even though the models in Figure 9.7a are realistic enough for visual identification, they differ from the

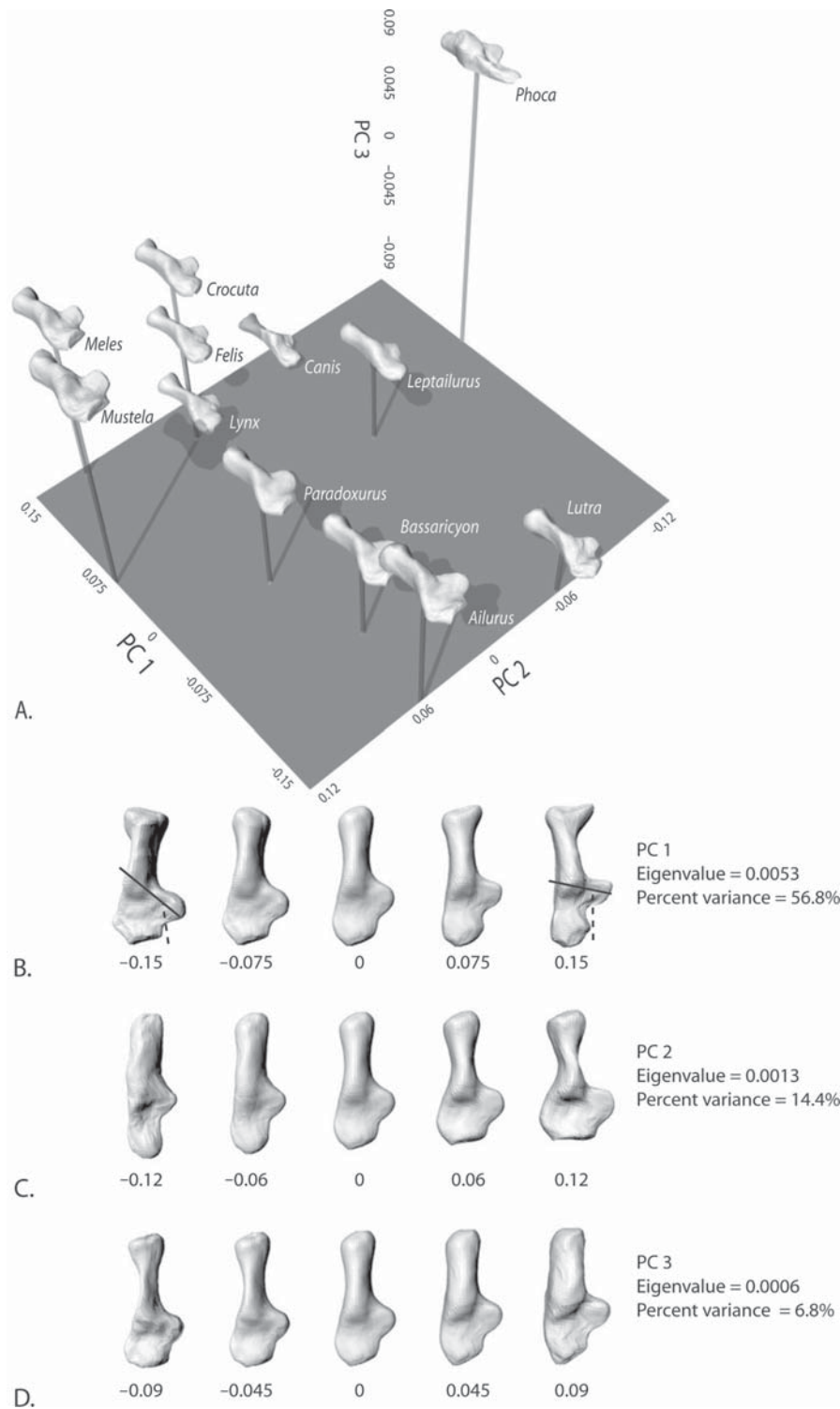


FIGURE 9.7. Principal components analysis of calcaneal shape. A, Ordination on the first three PCs. Taxa are represented by shape models constructed from their scores on all three axes. B, Shape models showing variation along PC 1. The position of each model is indicated by the number below it. An important part of variation on PC 1 is the orientation of the two facets (unbroken line) and the astragalar neck (broken lines), the curvature of the calcaneoastagalar facet, development of the peroneal tubercle, dominance of the lateral and medial calcaneal tubercles, and angle of the cuboid facet relative to the long axis of the bone. C, Shape models along PC 2. Important variation is width of the distal calcaneum, proximodistal position of the sustentacular process, and development of the calcaneal tubercle as a whole. The negative end of the axis is dominated by *Phoca*. D, Shape models along PC 3. Important variation includes shape of the calcaneoastagalar facet, development of the peroneal tubercle, and thickness of the calcaneal process. The positive end is dominated by *Phoca*.

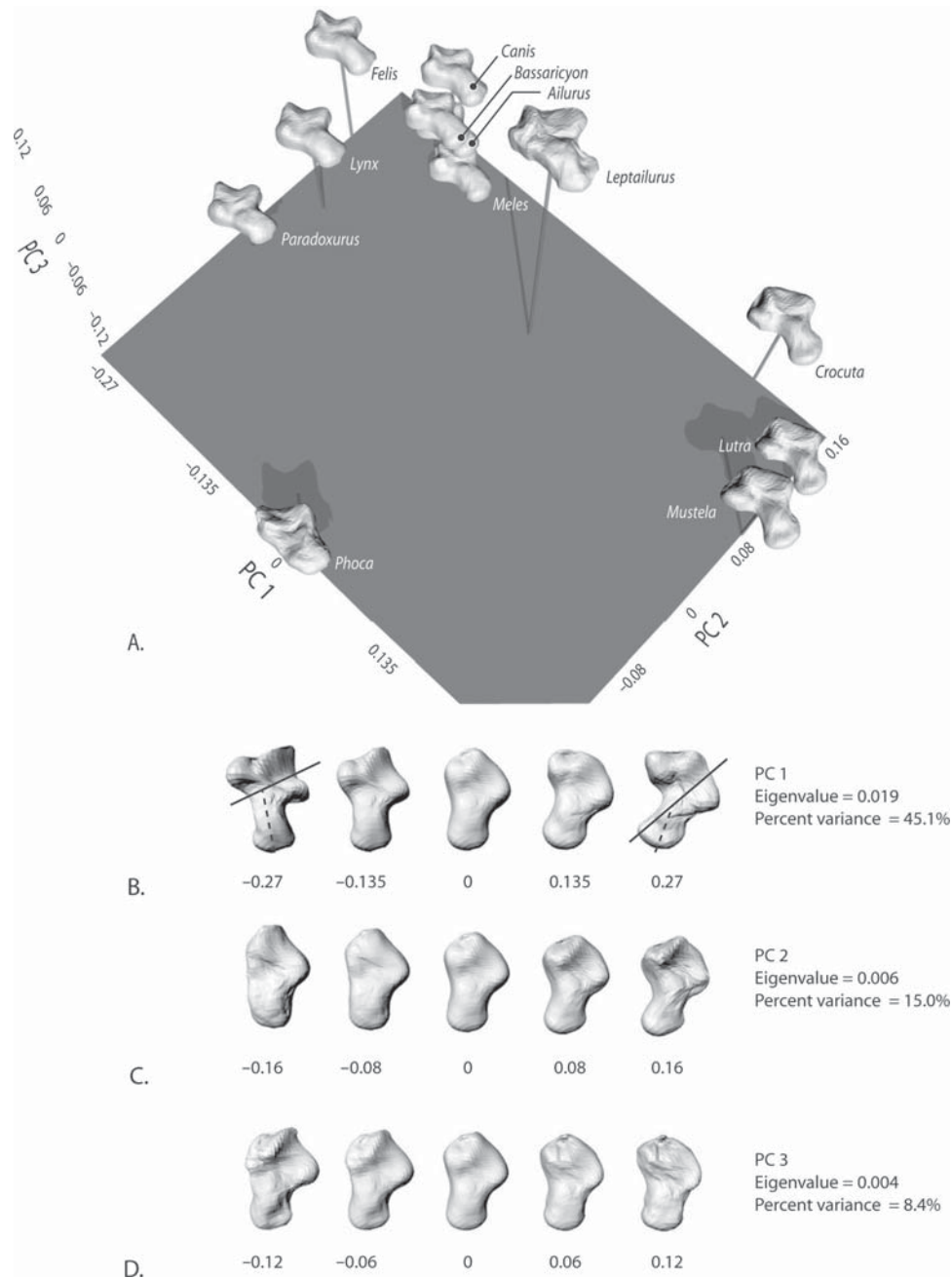


FIGURE 9.8. Principal components analysis of astragalar shape. A, Ordination of the first three PCs. B, Shape models along PC 1. Dominant variation is the orientation of the two facets (unbroken line) relative to the neck (broken line) and curvature of the calcaneoastagalar facet. C, Shape models along PC 2. Important variation is size of the proximal bony process (found only in phocids), length of the sustentacular facet, and the orientation and thickness of the neck. The negative end of the axis is dominated by *Phoca*. D, Shape models along PC 3. Important variation is plantar extension of the astragalar trochlea.

actual bones because PCs four through 11 were not included in their construction. If scores from all 11 PCs had been used, then the models would be indistinguishable from the original scans after interpolation.

### 9.3.2.1 Calcaneum

*PC 1.* The first principal component separated species by the orientation of the sustentacular facet, the dominance of

the lateral and medial calcaneal tubercles, development of the peroneal tubercle, width of the distal calcaneum, and angle of the cuboid facet relative to the long axis of the bone. The negative end of the axis – dominated by *Lutra*, *Ailurus*, and *Bassaricyon* – combined a distally positioned, dorsally facing sustentacular facet; a broadly curved calcaneoastagalar facet; a large lateral calcaneal tubercle; a large peroneal tubercle; a broad distal calcaneum; and a medially

angled cuboid facet. This morphology is associated with a mobile, plantigrade, five-digit foot. The narrowly acute angle between the line connecting the two facets and the main axis of the bone and the broad curvature of the calcaneoastagalgar facet are functionally associated with the ability to rotate the calcaneum under the astragalus for foot inversion (Szalay and Decker, 1974; Jenkins and McClearn, 1984). The strong peroneal process is probably associated with abduction of the fifth digit and eversion of the foot, because the tendons of the abductor digiti quinti and peroneus brevis pass under the process (Greene, 1935; Szalay, 1977a; Evans, 1993). The length of the calcaneal process gives these species a mechanical advantage for plantar flexion, a motion important in both swimming and climbing.

The positive end of the axis – dominated by *Crocota*, *Canis*, *Felis*, *Lynx* – combined a proximally positioned, distally facing sustentacular facet, a narrowly curved calcaneoastagalgar facet, a long, narrow distal calcaneum, a short peroneal process, a distally angled cuboid facet, a deep groove for the gastrocnemius tendon, and strong development of the medial calcaneal tubercle. This morphology is associated with a parasagittally constrained, digitigrade, four-digit foot. The proximal position of the sustentaculum and the narrowly curved calcaneoastagalgar facet restrict movement between the calcaneum and astragalus and help transmit weight straight down the shaft of the foot (Howell, 1944). The distally directed cuboid facet also transmits weight down the center axis of the foot. The proportionally long distal end of the calcaneum lengthens the moment arm of effort, emphasizing speed over strength during plantar flexion. *Meles* and *Mustela*, which do not have digitigrade, four-toed feet, also lay at the positive end of PC 1, but many of the features associated with that part of the axis are counteracted by the contribution of PC 2.

PC 1 is functionally associated with mobility in the LAJ and TTJ. This can be seen by following the axes of rotation of the upper ankle, lower ankle, and transverse tarsal joints through the series of models in Figures 9.7b and 9.8b. The upper ankle joint moves by rotation of the dorsal astragalgar trochlea against the tibia and fibula, roughly perpendicular to the hashed line. The lower ankle joint moves by rotation of the calcaneum under the astragalus along the axis represented by the solid line. The transverse tarsal joint moves by rotation of the cuboid and navicular against the facets on the distal end of the calcaneum and astragalus. Angles of the axes are functionally correlated because they are related both to the flexibility of the ankle and the type of stance (Schaeffer, 1947; Szalay and Decker, 1974; Decker and Szalay, 1974). Species at the negative end have greater mobility in the LAJ and TTJ and species at the positive end have less.

PC 2. The second principal component separated species on the shape of the calcaneal tuber, the width and shape of the distal calcaneum, and the position of the sustentaculum. The positive end of PC 2 – dominated by *Mustela* and *Meles* – paralleled the negative end of PC 1, but with a distally directed cuboid facet, a more narrowly curved calcaneoastagalgar

facet, and a more strongly developed medial calcaneal tubercle. This morphology is associated with a semidigitigrade, five-digit foot. The narrow curvature of the calcaneoastagalgar facet and the distally directed cuboid facet transmit weight associated with an upright stance.

The negative end of PC 2 – dominated by *Phoca* – combined a narrow calcaneal tubercle, narrow distal calcaneum, and a pointed, proximally positioned sustentaculum. At its extreme end, the axis is associated with the aquatic specializations found in pinnipeds, but towards the center it is associated with the more extreme cursorial specializations of *Canis* and *Leptailurus*, including a long, narrow calcaneum whose lever mechanics are optimized for speed over strength in plantarflexion.

PC 3. The third principal component separated species on the thickness of the calcaneal process and the orientation of the calcaneoastagalgar and cuboid facets. The positive end is dominated by *Phoca* and provides the oblique angle of its calcaneoastagalgar facet in combination with a proximally placed sustentaculum (an oblique angle is also found at the negative end of PC 1, but there it is associated with a distal sustentaculum). PC 1 also contributes further to the pointed distal end of *Phoca*'s calcaneum. The negative end of PC 3 is dominated by *Canis* and *Lynx*, which have a narrow calcaneal process shaft with a wider tuber at the end.

### 9.3.2.2 Astragalus

PC 1. The first astragalgar principal component separated species by the angle of the neck relative to the axis connecting the sustentacular and calcaneoastagalgar facets, and by the development of the medial trochlear ridge. The positive end of the axis – dominated by *Mustela*, *Lutra*, and *Crocota* – combined a narrow angle between neck and the axis connecting the two facets with a proximally prominent medial trochlear ridge. While part of this morphology parallels the positive end of the calcaneal PC 1, the taxa found at the positive end of the astragalgar axis share no special locomotor or phylogenetic similarity.

The negative end – dominated by *Felis*, *Lynx*, and *Paradoxurus* – combined a deep but rounded calcaneoastagalgar facet, a perpendicular angle between the neck and the axis connecting the sustentacular and calcaneoastagalgar facets, and a trochlea dominated by the lateral ridge. The animals at the negative end are the scansorial and arboreal feliform species.

PC 2. The second principal component is dominated by *Phoca* and separated species on the curvature of the calcaneoastagalgar facet, the length of the sustentacular facet, and the thickness of the neck.

PC 3. The third principal component is described a contrast between *Leptailurus* and *Meles*, separating species based on the curvature of the calcaneoastagalgar facet and the shape of the trochlea. The positive end of the axis represents a twisted calcaneoastagalgar facet, which faces laterally at the proximal end and ventrally at the distal end. This is combined with

a dominant lateral trochlear ridge with sharp plantar relief. *Leptailurus*, *Crocota*, *Canis*, *Felis*, and *Lynx*, all digitigrade species, lie towards the positive end of the axis.

The negative end of the axis represents calcaneoastragalar facet that faces ventrally along its entire length. The entire plantar surface of the astragalus has uniform, low relief. The arboreal and semifossorial species lie at the negative end.

### 9.3.3 Body Mass and Tarsal Shape

Body mass ( $\text{Log}_e$ ) and multidimensional calcaneum shape were not significantly related (MANOVA: Wilk's Lambda = 0.114,  $F_{10,1} = 0.777$ ,  $p = 0.716$ ), but body mass was significantly related to PC 2 individually (ANOVA:  $F_{1,10} = 11.43$ ,  $p = 0.007$ ). PC 2, which describes the width of the tuber, distal calcaneum, and position of the sustentacular facet, was dominated by *Phoca*, the largest species in the analysis. When *Phoca* was excluded, none of the individual calcaneum PCs is significantly related to body mass. Body mass was not related to astragalar shape, neither multidimensionally (MANOVA: Wilk's Lambda = 0.041,  $F_{10,1} = 2.341$ ,  $p = 0.472$ ) nor to individual PCs with or without *Phoca*.

### 9.3.4 Locomotion and Tarsal Shape

Calcaneum shape differed among locomotor types (Figure 9.9a). Semifossorial and natatorial calcanea were similar in the size and shape of their peroneal process and the position of their sustentaculum, but differed in the proportional length of the calcaneal process. Arboreal, scansorial, terrestrial and aquatic mean shapes were unique. Not only was shape significantly associated with locomotor type (Wilk's Lambda = 0.000,  $F_{30,6} = 12.12$ ,  $p = 0.002$ ), but 64.8% of the total shape variation could be explained by it. Locomotor diversity was most closely associated with PC 1, which was the only axis that individually had a statistically significant relation to locomotion ( $F_{5,6} = 6.98$ ,  $p = 0.017$ ). PC 1 described the position of the sustentaculum, the curvature of the calcaneoastragalar facet, the size of the calcaneal and peroneal tubercles, the width of the distal calcaneum, and the angle of the cuboid facet, features classically linked with locomotion because they influence the mobility, especially the rotation, of the ankle (Szalay, 1977a; Jenkins and McClearn, 1984). Locomotor mode explained 85% of the variation on PC 1.

Calcaneum shape was less influenced by stance, though averages of each of the three stance types were visibly different (Figure 9.9b). Digitigrade species shared a sharply convex calcaneoastragalar facet, a small peroneal process, and a proximally positioned sustentaculum. Plantigrade species shared a rounded calcaneoastragalar facet, a long peroneal process, and a larger, distally positioned sustentaculum. Semidigitigrade species were intermediate. As a whole, the association between stance and shape was not statistically significant (Wilk's Lambda = 0.000,  $F_{24,8} = 5.50$ ,  $p = 0.07$ ),

even though 46% of the total shape variation was explained by stance. Correlation of stance with PC 2 was significant, however ( $F_{3,8} = 4.21$ ,  $p = 0.046$ ). The second PC describes correlations in the width of the distal calcaneum, the width of the tuber, and the position of the sustentaculum. Narrower distal calcanea result from a narrower peroneal process and cuboid facet, both associated with reduction in the number of digits, which itself is associated with digitigrady. The sustentaculum is also more posteriorly positioned in digitigrade species.

Calcaneum shape was also only marginally influenced by the number of toes (Figure 9.9c). The mean calcaneal shape of five-digit species had a rounded calcaneoastragalar facet, an open, distally positioned sustentaculum, an angled cuboid facet, a medium-sized peroneal process, and a relatively short calcaneal process. Four digit species had a more sharply curved calcaneoastragalar facet, a more posteriorly positioned sustentaculum, a narrower, more sharply defined peroneal process, and a longer calcaneal process. The difference was not significant (Wilk's Lambda = 0.012,  $F_{10,1} = 8.34$ ,  $p = 0.26$ ), though digit number was significantly related to PC 1 by itself ( $F_{1,10} = 6.49$ ,  $p = 0.029$ ). Digit number and locomotor type are themselves correlated, with four-digit species dominating the scansorial and terrestrial types.

Astragalus shape was associated with locomotor type (Figure 9.9d). Arboreal astragali were characterized by long necks, large sustentacular facets, and open calcaneoastragalar facets. Scansorial species had shorter necked astragali. The sustentacular facets of terrestrial species were smaller, and their calcaneoastragalar facets more sharply concave. Semifossorial taxa had blockier with a more angled trochlea, while natatorial astragali (represented only by *Lutra*) had a very long calcaneoastragalar facet compared to the neck. Aquatic astragali (represented only by *Phoca*) had a very thick neck, large sustentacular and calcaneoastragalar facets, and no ventral extension of the trochlea. Differences among locomotor types were significant (Wilk's Lambda = 0.000,  $F_{30,6} = 7.75$ ,  $p = 0.008$ ), with PC 5 having the strongest association ( $F_{5,6} = 6.37$ ,  $p = 0.022$ ); 62.3% of shape variation was explained by locomotor type.

Stance had a significant effect on astragalus shape (Figure 9.9e). Digitigrade species had sharply curved calcaneoastragalar facets, semidigitigrade taxa had more open ones, and plantigrade species had long, narrow necks. The difference among stance categories was significant (Wilk's Lambda = 0.000,  $F_{24,8} = 20.78$ ,  $p = 0.01$ ), with PC 2 having the strongest association ( $F_{3,8} = 6.91$ ,  $p = 0.013$ ).

Astragalus shape was not significantly related to digit number (Figure 9.9f). Five digit species had a flatter calcaneoastragalar facet and a narrower distal trochlea, while four digit species had a blockier body and anteriorly directed neck. The differences were not significant (Wilk's Lambda = 0.003,  $F_{10,1} = 30.12$ ,  $p = 0.141$ ), though digit number was significantly related to PC 3 by itself ( $F_{1,10} = 11.42$ ,  $p = 0.007$ ).

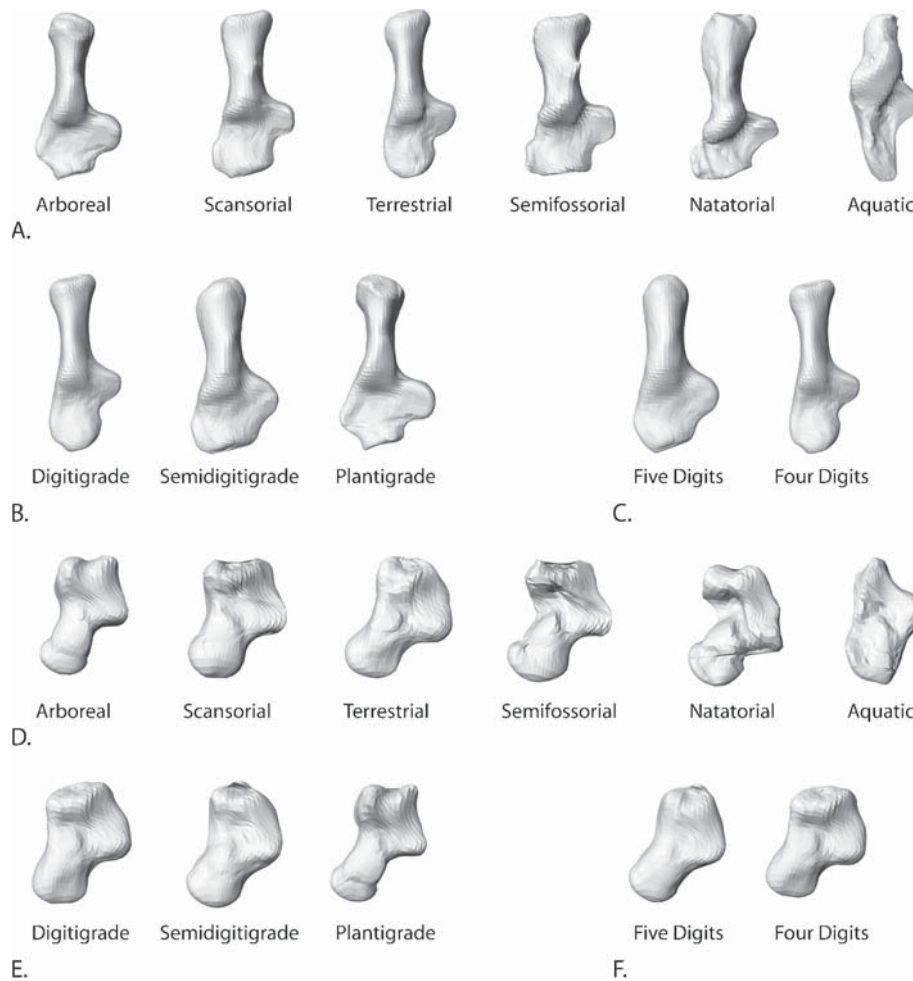


FIGURE 9.9. Mean tarsal shape for different locomotor categories. A, Mean calcaneum shape for the six locomotor types. Differences among types are significant ( $p < 0.01$ ). B, Mean calcaneum shape for the three stance types. Differences are not significant ( $p = 0.07$ ; but see text). C, Mean calcaneum shape for four and five digit species. Differences are not significant ( $p = 0.26$ ; but see text). D, Mean astragalar shape for the six locomotor types. Differences are significant ( $p < 0.01$ ). E, Mean astragalar shape for the three stance types. Differences are significant ( $p < 0.01$ ). F, Mean astragalar shape for four and five digit species. Differences are not significant ( $p = 0.14$ ).

### 9.3.5 Locomotion and Facets

Occluding facets are expected to have different areas and curvatures. Joints with greater mobility should have greater disparity in size and curvature than those with less (MacConaill, 1946a, b, c; Szalay and Drawhorn, 1980; Szalay, 1994). Surprisingly, neither facet area nor curvature was correlated with locomotor type in these carnivores (Table 9.2, Figure 9.10).

Locomotor type and sustentacular facet area index – the proportion of the larger to smaller facet – were not significantly correlated ( $F_{5,6} = 0.82$ ,  $p = 0.58$ ). *Lutra*, *Bassaricyon*, and *Ailurus* had the biggest difference in facet size, while *Crocota*, *Paradoxurus*, and *Phoca* had the smallest. In all species except *Phoca*, the calcaneum had the largest of the two sustentacular facets, probably because in fissipeds the concave shape of the lower facet supports weight and constrains translation of the astragalar neck (Figure 9.10a).

The size of upper and lower calcaneoastragalar facets was also unrelated to locomotor type (Figure 9.10b). The statistical relationship was not significant ( $F_{5,6} = 2.41$ ,  $p = 0.16$ ) and there was no obvious phylogenetic relationship. *Canis*, *Felis*, *Crocota*, and *Phoca* had facets that were the most equal in size, and *Lutra* had the ones with the biggest difference. About half the taxa had a larger calcaneal facet, while the remaining had a larger astragalar one.

The sustentacular facet was more strongly curved on the astragalus than on the calcaneum in all species (Figure 9.10c). *Bassaricyon*, *Leptailurus*, and *Lynx* had curvatures that were most similar, while *Paradoxurus*, *Meles* and *Crocota* had the biggest difference. In *Paradoxurus* the curvature coefficient on the astragalus was especially large, 3.4 times greater than on the calcaneum. This value does not seem to be in error (the measurements and calculations were rechecked several times), but it does not correspond to any known locomotor peculiarity

TABLE 9.2. Area and curvature of the sustentacular and calcaneoastragalar facets on the astragalus and calcaneum. The index is the ratio of the larger over the smaller value for each facet (compare with plots in Figure 9.10).

Species	Area (mm <sup>2</sup> )						Curvature					
	Calcaneum		Astragalus		Index		Calcaneum		Astragalus		Index	
	Sust.	Calc-astr.	Sust.	Calc-astr.	Sust.	Calc-astr.	Sust.	Calc-astr.	Sust.	Calc-astr.	Sust.	Calc-astr.
<i>Ailurus</i>	2.59	3.77	3.24	3.62	1.25	1.04	0.040	0.092	0.066	0.065	1.64	1.41
<i>Bassaricyon</i>	2.37	3.11	3.07	3.32	1.30	1.07	0.043	0.088	0.050	0.074	1.16	1.19
<i>Canis</i>	3.81	5.25	4.07	5.25	1.07	1.00	0.025	0.086	0.035	0.098	1.40	1.14
<i>Crocota</i>	4.53	5.25	4.64	5.31	1.02	1.01	0.018	0.077	0.032	0.055	1.78	1.40
<i>Felis</i>	2.84	3.80	3.35	3.76	1.18	1.01	0.039	0.149	0.052	0.119	1.33	1.25
<i>Leptailurus</i>	3.29	4.25	3.92	4.57	1.19	1.08	0.034	0.119	0.041	0.105	1.21	1.13
<i>Lutra</i>	2.81	4.45	3.61	3.86	1.28	1.15	0.048	0.139	0.067	0.070	1.40	1.99
<i>Lynx</i>	3.43	4.39	4.03	4.54	1.17	1.03	0.029	0.081	0.036	0.079	1.24	1.03
<i>Meles</i>	2.90	4.53	3.16	4.32	1.09	1.05	0.037	0.061	0.069	0.044	1.86	1.39
<i>Mustela</i>	1.50	2.85	1.90	2.63	1.26	1.09	0.069	0.201	0.090	0.169	1.30	1.19
<i>Paradoxurus</i>	2.81	3.47	3.05	3.32	1.09	1.04	0.035	0.093	0.119	0.056	3.36	1.67
<i>Phoca</i>	4.71	4.89	4.46	4.99	1.06	1.02	0.018	0.047	0.028	0.043	1.56	1.10

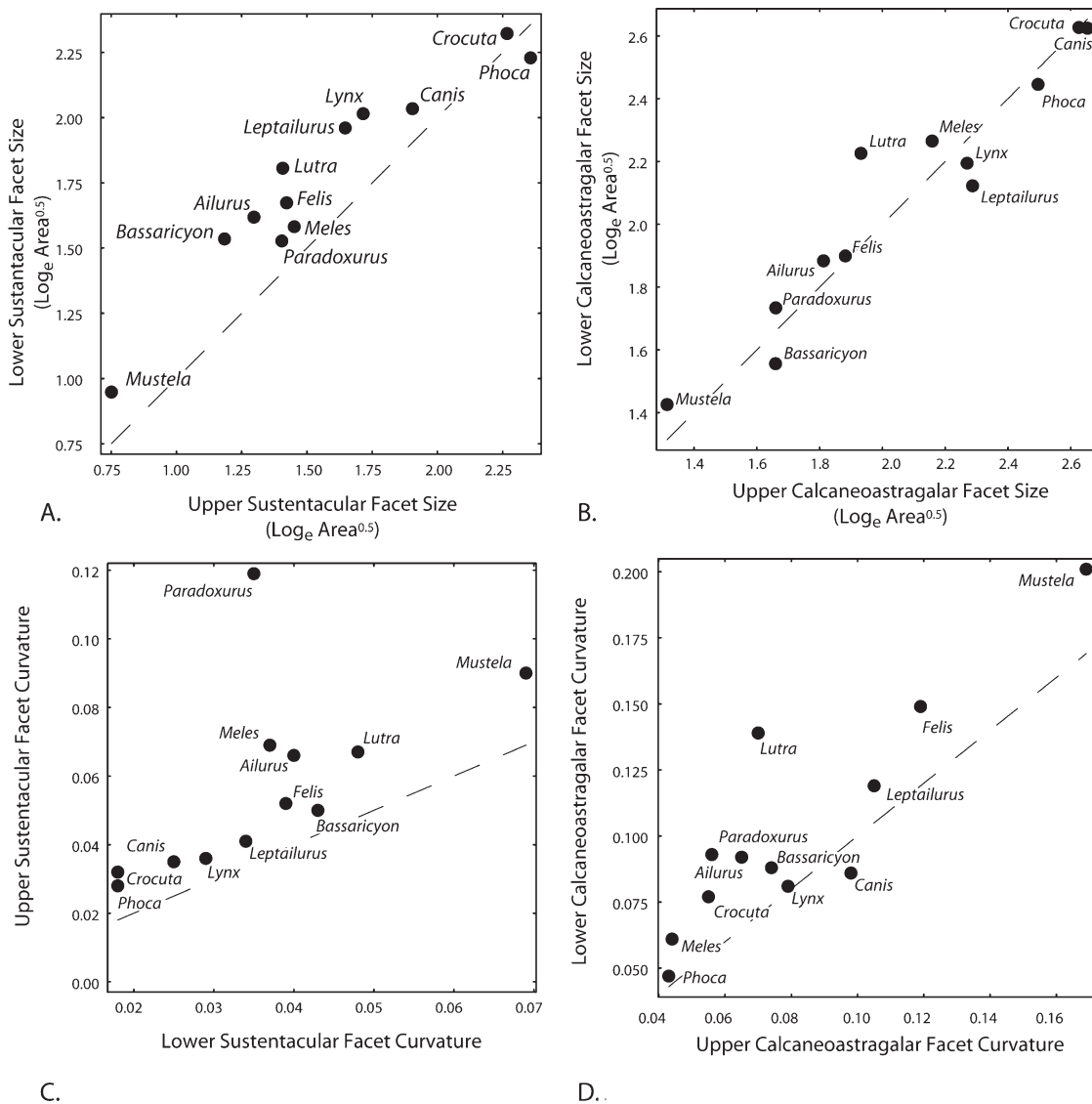


FIGURE 9.10. Area and curvature of occluding astragalar and calcaneal facets. A, Upper (astragalar) and lower (calcaneal) sustentacular facet size. B, Upper and lower calcaneoastragalar facet size. C, Upper and lower sustentacular facet curvature. D, Upper and lower calcaneoastragalar facet curvature. In each plot, the broken line shows a 1 to 1 relationship. The area plots use the natural logged square root of the measurements reported in Table 9.2. The curvature plots use the same values as Table 9.2.

of the animal. The large value may result from non-linearity in the curvature coefficient that could be compensated for by transformation before the calculation of ratios, but data were not available to assess this possibility. The *Paradoxurus* specimen was also from a relatively young animal, which could also explain the large difference in curvature between the two facets. There was no significant statistical relationship between curvature and locomotor mode ( $F_{5,6} = 0.44$ ,  $p = 0.80$ ).

Curvature in the calcaneoastragalar facets was greater on the calcaneum in all taxa except *Canis* (Figure 9.10c). *Lutra*, *Paradoxurus*, and *Ailurus* had the biggest difference in curvature, while *Lynx*, *Phoca*, and *Leptailurus* had the smallest. There was no statistical relationship between curvature and locomotor type for this facet either, though the association was stronger than for the sustentacular one ( $F_{5,6} = 4.08$ ,  $p = 0.06$ ).

These results suggest that mobility is constrained by something other than differences in curvature between occluding facets. The overall curvature of the joint, as opposed to the difference between its facets, is unquestionably related to mobility. The cartilaginous joint surfaces, which were not measured in this study, may also introduce differences in occluding facet curvature.

### 9.3.6 Body Mass and Facets

The area of all four facets was significantly related to body mass (Sustentacular: Calc,  $F_{1,10} = 109.23$ ,  $p < 0.01$ ; Astr,  $F_{1,10} = 34.84$ ,  $p < 0.01$ . Calcaneoastragalar: Calc,  $F_{1,10} = 49.59$ ,  $p < 0.01$ ; Astr,  $F_{1,10} = 49.78$ ,  $p < 0.01$ ). Larger species had bigger facets. The index of proportional size was significantly related to body mass for the sustentacular facets ( $F_{1,10} = 12.72$ ,  $p < 0.01$ ). Larger species had sustentacular facets of similar size, while smaller species had proportionally larger sustentacular facets on the calcaneum. Body size was not related to the index of proportional size for the calcaneoastragalar facets ( $F_{1,10} = 2.26$ ,  $p = 0.16$ ).

Curvature was related to body mass for only some facets. The relation was significant for both sustentacular facets (Calc,  $F_{1,10} = 25.56$ ,  $p < 0.01$ ; Astr,  $F_{1,10} = 7.36$ ,  $p = 0.02$ ) and for the calcaneal calcaneoastragalar facet ( $F_{1,10} = 7.32$ ,  $p = 0.02$ ), but not for the astragalar calcaneoastragalar facet ( $F_{1,10} = 3.99$ ,  $p = 0.07$ ). All facets were less curved in larger species. The index of curvature was not related to body mass for either facet.

### 9.3.7 Correlation Between Calcaneum and Astragalus Shape

The calcaneum and astragalus are functionally integrated, especially at the synovial joint contacts. During the course of evolution, the position, size and shape of the facets must change together or the joint will not work. The PCAs identified major axes of variation, but those results cannot reveal anything about correlations between the bones. 2B-PLS was used to identify correlated variation in the calcaneum and astragalus.

This method is similar to PCA in that it extracts a series of axes explaining shape variation but, unlike PCA, 2B-PLS finds axes of correlation between the two shapes. The results of a 2B-PLS analysis of calcaneum and astragalus shape are shown in Figure 9.11. Each PLS axis explains a certain percentage of the total covariation between the two bones, with the first axis explaining the most. Each axis has two vectors, one for each bone. Shape models along the two vectors illustrate variation correlated between the bones. Correlation in real species is usually not 100% and a perfect correlation would be represented on each plot by a diagonal line with a slope of one. Real data are scattered around that line, indicating residual variation in one or both of the bones that cannot be explained by the PLS axis. Each axis therefore has a correlation coefficient ( $R$ ) that describes the strength of the correlation on that axis.

PLS 1 described correlation between the angles of the transverse tarsal joint and the lower ankle joint (Figure 9.11a). This axis explained 24.5% of the covariation between the two bones. On the calcaneum, the correlated variation included the orientation of the sustentacular facet, the angle of the calcaneoastragalar facet, the depth of the groove for the peroneus brevis, and the angle of the cuboid facet relative to the long axis of the bone. These features were correlated on the astragalus with the angle of the calcaneoastragalar facet to the neck, the blockiness of the body, and the relative size of the proximal trochlear ridges. The correlation coefficient ( $R$ ) for the two bones on PLS 1 was 0.79. Note that neither PLS vector was exactly like any PC in Figure 9.7 or 9.8. The calcaneum PLS 1 was most similar to calcaneum PC 3, but contained some aspects of PC 1. Astragalus PLS 1 was a combination of PCs 1 and 2. The reason that PLS and PC axes were not identical was that part of the variation in either bone is not correlated with variation in the other. This bone-specific variation does not appear on any of the PLS axes, but it may contribute heavily to PC axes.

PLS 2 described the proximodistal position of the sustentacular facet (Figure 9.11b). PLS 2 explained 18.4% of the covariation. On the calcaneum this was manifested in the position of the sustentacular process and the width of the distal calcaneum and on the astragalus it was manifested in the length and angle of the neck. The calcaneum PLS vector closely resembled calcaneum PC 2, but the astragalus PLS vector was not really like any of its PC axes. Correlation between the two bones on PLS 2 was 0.90. PLS 2 has a strong functional component. With arboreal *Ailurus* and *Bassaricyon* at one end and aquatic *Phoca* at the other, the axis forms a transect from arboreal through natatorial, semiplantigrade terrestrial, scansorial, digitigrade cursorial, to aquatic.

PLS 3 and 4 explained 14.8% and 10.4% respectively, with correlation coefficients of  $R = 0.77$  and  $R = 0.83$ . Readers can see for themselves the shape associated with each in Figure 9.11c and 9.11d.

### 9.3.8 Evolution of Tarsal Morphology

The fossil record yields the only direct data about morphologies and locomotor specializations in the past, but phylogenetic

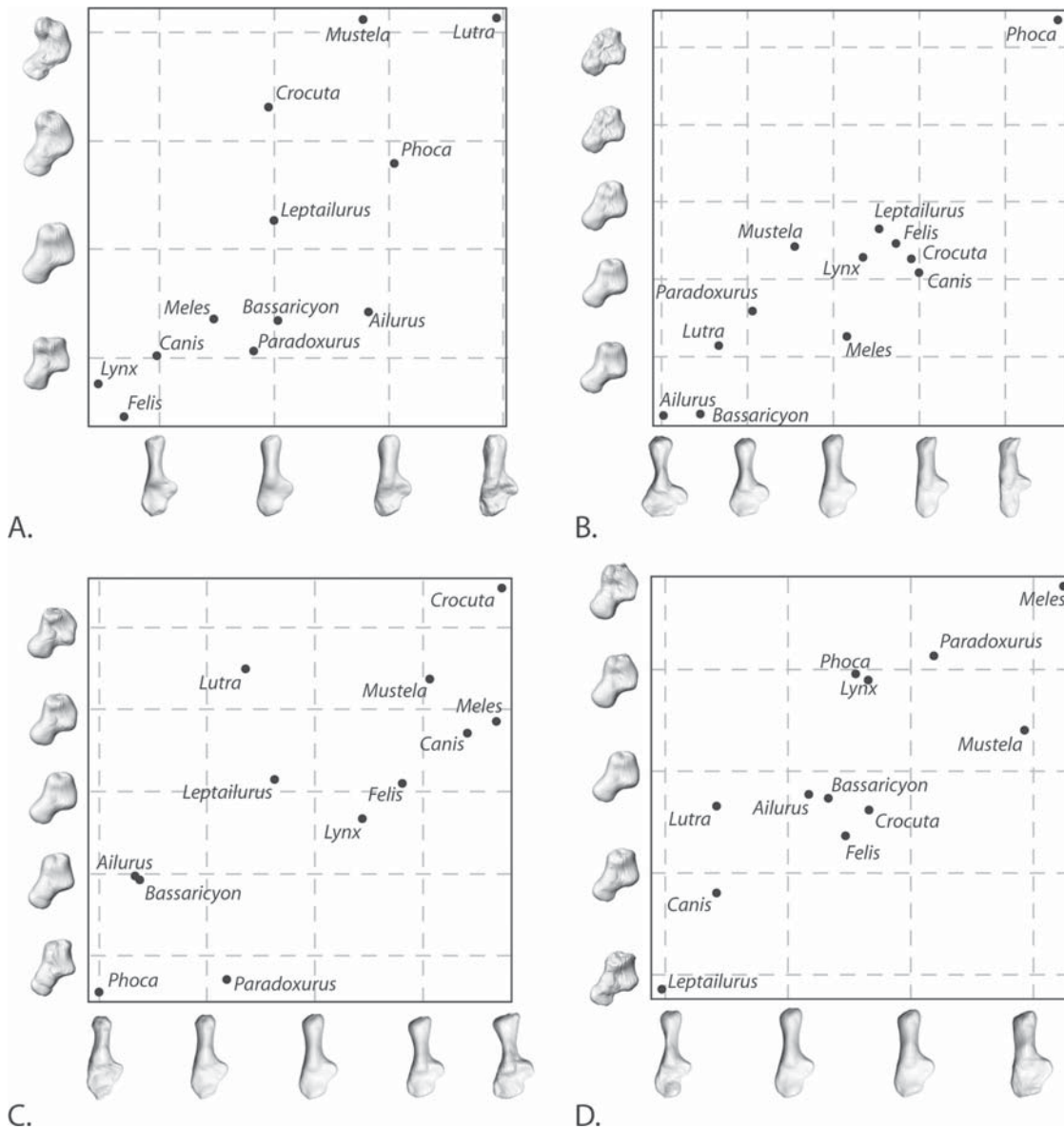


FIGURE 9.11. Correlation of calcaneum and astragalus shape 2B-PLS results. A, Axis 1. B, Axis 2. C, Axis 3. D, Axis 4. Each PLS axis has two vectors so that each graph has the calcaneum as its abscissa and the astragalus as its ordinate. The shape transformation along the vectors is shown as a series of models.

comparative analysis of living taxa can be used to make indirect inferences, inferences which can later be tested against palaeontological evidence. In this section, ancestral reconstructions of tarsal shape are presented, ancestral functional conditions are estimated by quantitative comparison of the reconstructions to the models in Figure 9.9, and the existence of an adaptive zone is tested (1) by projecting the phylogenetic tree back into the morphospace to look for boundaries and convergence; (2) by testing shape divergence relative to recency of common ancestry for saturation; and (3) by comparing terminal outliers to branching pattern and to ecological changes. A tree is also constructed from tarsal shape for comparison to the established phylogenetic tree.

Ancestral reconstructions and locomotor interpretations are shown in Figure 9.12. Only one reconstruction is shown for the multiple branching events at Nodes 1, 4, and 5 because those splits were spaced too closely in time to be separated paleontologically (Flynn, 1996). Node reconstructions are identical if the branching events are not separated in time. The shape at Node 3 is not shown because it was not visibly different from Node 2. The reconstructions were based on the 11 PC axes for each bone. Shapes were also reconstructed from the PLS axes, which maximize the correlation between the two bones, but they were not different than the ones shown here and will not be considered further. The reconstructions are the most parsimonious shapes for

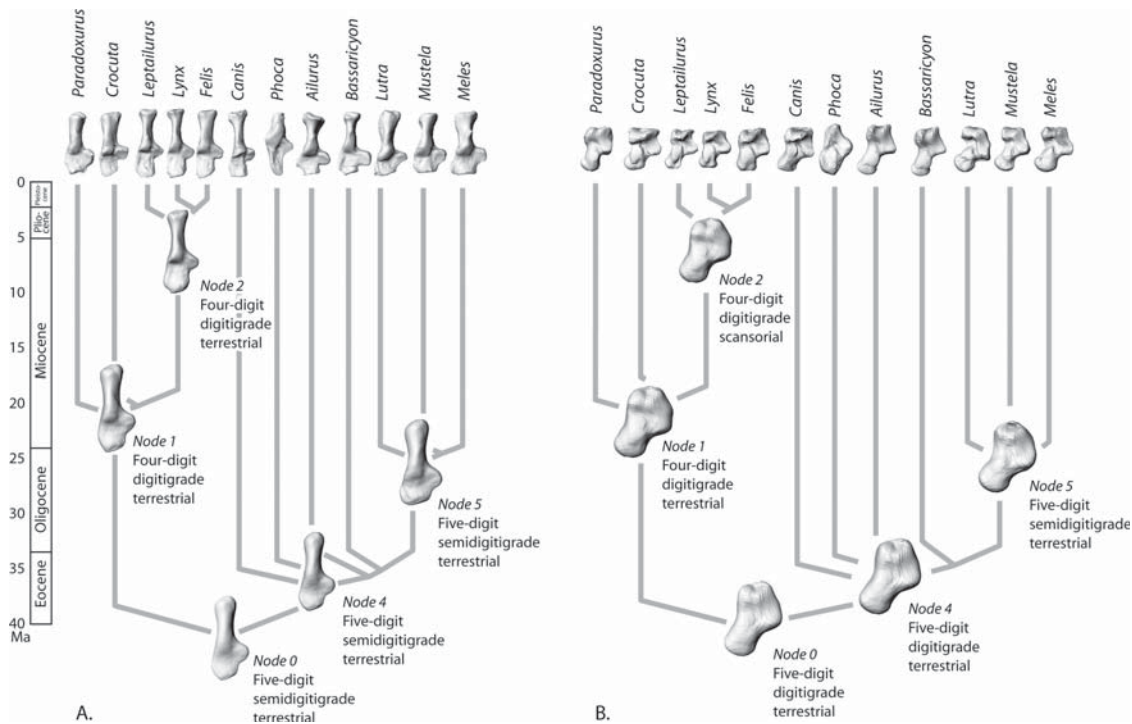


FIGURE 9.12. Ancestral node reconstructions based on the tree in Figure 9.5. A, Calcaneum. B, Astragalus. Locomotor descriptions are from the best match between the reconstructions and the models in Figure 9.9. Tip shapes are shown for reference. Node 3 is not shown because of its similarity to Node 2.

the tarsals using a likelihood model that assumes that the tree and its branch lengths are correct, assumes a Brownian motion model of evolution (which may not be the case because evolution in carnivoran tarsals may be constrained by an Ornstein-Uhlenbeck process, as discussed below), assumes that the shape of each species is accurately represented, and assumes that these taxa are representative of the true diversity of the group. Even though the reconstructions presented here are the most likely given the data, many other ancestral shapes may be nearly as likely (Martins and Hansen, 1997; Garland and Ives, 2000; Polly, 2001). The relative support for other hypotheses, such as independently observed fossil morphologies, can, in principle, be judged using log-likelihood ratios, but such tests were not attempted here because they are tangential to the main purpose of the paper.

The calcaneum and astragalus reconstructions at the base of the tree (Node 0) and at the base of the caniniform clade (Node 4) were similar, in part because of the short temporal interval between them. Both shapes were interpreted as belonging to five-digit terrestrial species by finding the closest match among the locomotor models in Figure 9.9. The interpretation of stance differed in the two bones, with the calcaneum most closely matching the semidigitigrade mean and the astragalus matching the digitigrade one. The match is closer in the calcaneum, lending support to the semidigitigrade hypothesis, but differences among stance

categories were more significant in the astragalus, lending contradictory support to the digitigrade hypothesis. These reconstructions are consistent with two previous hypotheses of a terrestrial ancestry for carnivorans, one based on eutherian mammals in general (Szalay, 1977a, 1984) and the other on the early carnivoran *Didymictis* (Heinrich and Rose, 1997). The ancestral shape of Mustelidae (Node 5) had a longer peroneal process on the calcaneum and a more trapezoidal body shape on the astragalus. The locomotor reconstruction was five digit, semidigitigrade terrestrial for both calcaneum and astragalus. The reconstruction at the base of the feliform clade (Node 1) was similar to the earliest carnivoran ancestor, but with a shorter distal calcaneum and blockier astragalus body. Both bones suggested a four digit, digitigrade, terrestrial ancestor. If this is correct, then the five digit condition of some viverrids and herpestids may be an evolutionary reversal, a scenario already feasible because of the variation in digit number among these groups and disagreements about their phylogeny (Taylor, 1970, 1976, 1988; Veron and Heard, 2000; Gaubert and Veron, 2003). The felid ancestor was the most visibly different, with a dainty peroneal process and a proximally placed sustentaculum. Both bones suggested a terrestrial locomotor mode while the astragalus a scansorial one, an ambiguity contributed by the specializations of *Leptailurus*.

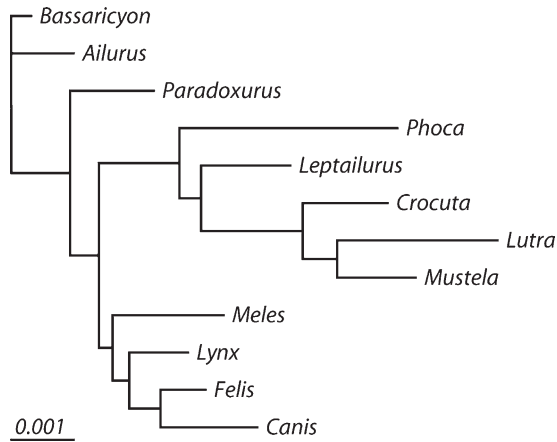


FIGURE 9.13. A maximum likelihood tree constructed from calcaneum and astragalus shape. The groupings are influenced by low-level phylogenetic relationship and locomotor type, but do not clearly indicate either.

The similarity among the reconstructed nodes and the diversity among the tips suggest considerable homoplasy in shape. I tested this first by building a maximum-likelihood tree from combined calcaneum and astragalus shape scores (Figure 9.13). This tree had a log likelihood of 600.1. Comparison with Figures 9.7 and 9.8 shows that the topology is influenced mostly by the astragalus. *Lutra*, *Mustela*, and *Crocuta*, which are united in the tree, are closely clustered in the astragalus PC plot, but not so in the calcaneum one. The groupings in the tree are not phylogenetic, but neither do they appear to be functional; they are a compromise between the two, and between the conflicting signals from the two bones. The lack of clear phylogenetic signal has two causes: (1) considerable shape convergence among the fissipeds has arisen because of their long history within a constrained adaptive zone, and (2) *Phoca*, which has escaped from that adaptive zone, has an especially different shape branch, preventing it from being sensibly grouped with the fissipeds.

The extent of the homoplasy, the outlines of the fissiped adaptive zone, and the position of *Phoca* outside the adaptive zone are clear in Figure 9.14. The diagrams were made by projecting the ancestral node reconstructions into the shape space and connecting the branches of the tree. Terminal taxa are represented by large, labeled balls and nodes by small numbered ones. The phylogenetic pattern in the shape space is a tangled mess. Descendants of Node 5, for example, have colonized all extremes of both the calcaneum and astragalus shape space, and the same is true for Node 4. The immediate ancestors of *Paradoxurus* and *Bassaricyon* evolved in different directions from node 0, but then the terminal lineages moved in parallel, ending up with similar forms. Despite the chaos, the fissipeds were constrained within a limited area of the space, while *Phoca* followed a trajectory out of the tangle into a shape region of its own. These features fulfill the main criteria proposed above for the recognition of an adaptive zone: the zone is occupied, the zone has phenotypic limits that are associated with functional differences (the functional associations described

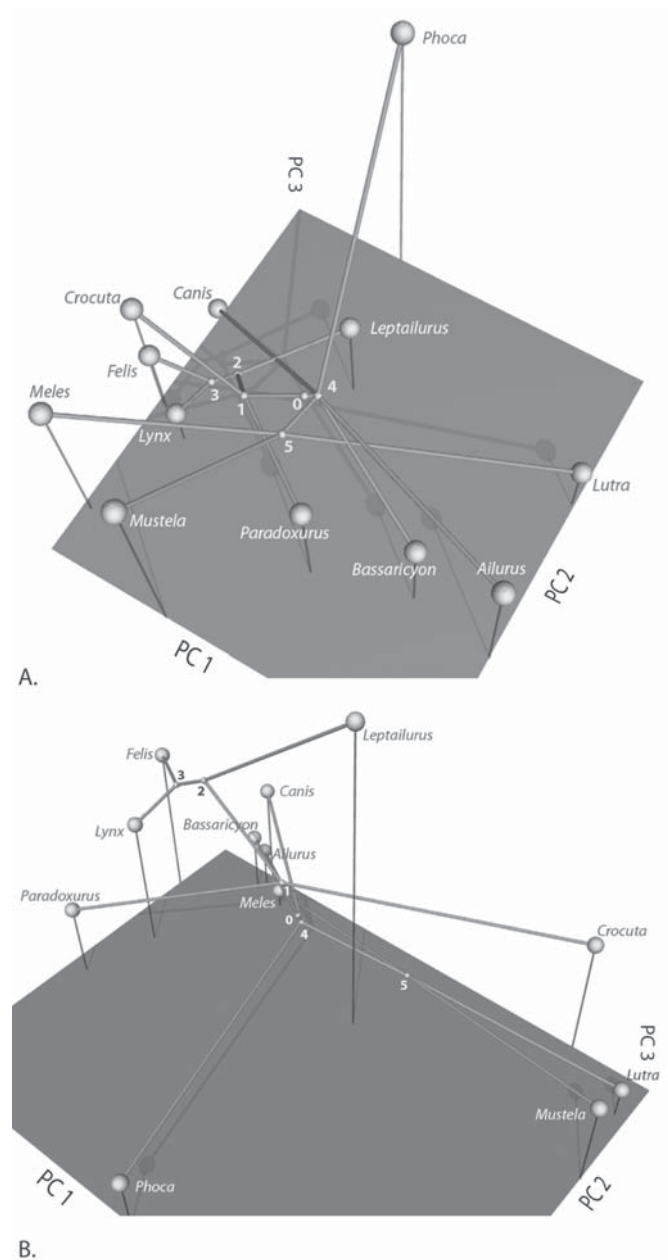


FIGURE 9.14. Tree projection into morphospace. A, Calcaneum. B, Astragalus. Node reconstructions from Figure 9.12 were projected into the PC spaces (Figures 9.7 and 9.8) and the branches connected. Node numbering follows Figure 9.5. Tarsal morphology crisscrossed the morphospace, erasing phylogenetic history as various locomotor types re-evolved in different clades. The branch leading to *Phoca* set off in a new direction not otherwise traversed.

above for the first three PC axes), phylogenetic history suggests that evolution beyond the boundaries was rare, and the only lineage to travel outside the boundaries evolved into a radically different functional context.

The interplay between rate of shape evolution, the boundaries of the adaptive zone, and recency of common ancestry are important for understanding homoplasy and phylogenetic signal. For most of these taxa, the rate was rapid enough and

common ancestry ancient enough for the ancestral condition not to be a good predictor of terminal shape. In other words, unrelated terminal taxa are likely to be more similar to one another than they are to their immediate ancestors. Node 5 is a good example. Descendants of that node have moved to three extremes in both shape spaces in only 24 million years. The rate of evolution is fast enough that any point in the fissiped adaptive zone can be reached from any other in much less time than the groups have been evolving. This situation makes convergent evolution highly probable. Only the felid clade has not diffused to the far corners. All three species occupy a relatively small proportion of both shape spaces. *Felis* and *Lynx* are closer to one another than they are to the more distantly related *Leptailurus* and subtending nodes 2 and 3 occupy phylogenetically logical positions. This is a recent clade, sharing its last common ancestor only 4.5 million years ago, a time too short to reach the boundaries of the adaptive zone. Note, however, that *Leptailurus* has moved nearly halfway across the space. Based on these observations, we can guess that good phylogenetic signal could be extracted when the last common ancestor is no more than 3–5 million years older than the taxa in question. Phylogenetic analysis based on tarsal shape would have to be confined to closely related taxa or have enough fossil taxa at intermediate ages to ensure that the longest branches are no more than a few million years long. This restriction only exists because of the boundaries of the adaptive zone. If evolution could continue indefinitely in any morphological direction, then homoplasy would be less likely because lineages would not have to double back in the morphospace. As long as the rate of evolution is slow enough, the adaptive boundaries broad enough, and the branch lengths short enough, phylogenetic reconstruction from morphological shape is possible.

Rates on the tree varied, but fell within an order of magnitude of one another. Rates were calculated by measuring shape change along each branch and divided by branch length scaled to generations. Branch lengths and rates along terminal branches are reported in Table 9.3. The highest rate was  $2.5 \times 10^{-8}$  Procrustes units/gen, measured in the astragalus of *Leptailurus*.

TABLE 9.3. Branch lengths and rates of shape change from terminal taxa to their immediately ancestral node. Branch lengths are in Procrustes units<sup>2</sup> and rates in Procrustes units<sup>2</sup> per generation.

Species	Calcaneum		Astragalus	
	Branch length	Rate	Branch length	Rate
Ailurus	0.021	$2.2 \times 10^{-9}$	0.018	$1.9 \times 10^{-9}$
Bassaricyon	0.014	$1.5 \times 10^{-9}$	0.017	$1.8 \times 10^{-9}$
Canis	0.019	$2.0 \times 10^{-9}$	0.026	$2.8 \times 10^{-9}$
Crocota	0.008	$1.4 \times 10^{-9}$	0.048	$8.3 \times 10^{-9}$
Felis	0.003	$3.3 \times 10^{-9}$	0.015	$1.6 \times 10^{-8}$
Leptailurus	0.007	$6.0 \times 10^{-9}$	0.029	$2.5 \times 10^{-8}$
Lutra	0.023	$3.7 \times 10^{-9}$	0.032	$5.0 \times 10^{-9}$
Lynx	0.004	$4.3 \times 10^{-9}$	0.009	$1.0 \times 10^{-8}$
Meles	0.009	$1.4 \times 10^{-9}$	0.068	$1.1 \times 10^{-8}$
Mustela	0.012	$1.9 \times 10^{-9}$	0.031	$5.0 \times 10^{-9}$
Paradoxurus	0.008	$1.3 \times 10^{-9}$	0.030	$5.2 \times 10^{-9}$
Phoca	0.026	$2.7 \times 10^{-9}$	0.050	$5.2 \times 10^{-9}$

The lowest rate was  $1.3 \times 10^{-9}$  in the calcaneum of *Paradoxurus*. The highest calcaneum rate was  $6.0 \times 10^{-9}$  in *Leptailurus*, and the lowest astragalus rate was  $1.8 \times 10^{-9}$  in *Bassaricyon*. Some of the highest rates were in the shortest branches, especially the felid ones. This distribution could be related to the scaling phenomenon of rate to interval, where shorter intervals yield higher rates all else being equal (Gingerich, 1993), but some of the highest rates (e.g., the rate of astragalus change in *Meles*) were associated with long branches.

The rates in *Phoca* were intermediate. Its calcaneum rate of  $2.7 \times 10^{-9}$  fifth highest, and its astragalus rate of  $5.2 \times 10^{-9}$  was sixth highest. Despite *Phoca* having traveled far beyond the boundaries of the fissiped adaptive zone, there is no evidence that it did so at a higher rate, contrary to the expectation of Simpson (1944, 1953) that crossing adaptive zone boundaries will be accompanied by an exceptionally high rate of change. The remarkable, derived morphology of *Phoca's* tarsals was not produced by evolving faster, but simply by evolving in a different direction than other fissiped taxa, following trajectories with different covariances, a situation in keeping with Hecht's (1965) view that seemingly rapid rates may result from morphologic reorganization. The choice of *Phoca* among the extant pinnipeds should not influence the conclusion drawn here, however. Because phocids have a more derived tarsal morphology than otariids or odobenids, the estimated rate of change will be maximized so that quantum evolution, if it were present, should be easily detectable using *Phoca*. But the rate calculated here was based on the amount of change between an extant species and a reconstructed ancestor. If fossil taxa were included, one might find a localized region of the pinniped clade which did experience rapid evolution.

The constraints on phylogenetic divergence can be measured a second way using the scaling of morphological divergence to time since common ancestry (Figure 9.15). The scaling relationship indicates whether the phenotype is evolving freely, whether it is constrained in how much it can change, or whether it is being pushed uniformly in a particular direction (Gingerich, 1993; Hansen and Martins, 1996; Polly, 2001, 2004; Roopnarine, 2001). When evolution is unconstrained and unbiased (i.e., Brownian motion), phenotypic divergence will increase with the square-root of time (it diverges linearly when measured in variance units); when the phenotype changes constantly in a single direction, such as under long-term directional selection, divergence will scale linearly with time; and when divergence is constrained, such as within an adaptive zone, it will reach a plateau with respect to time. These modes of evolution can be measured by regression fitting. For untransformed data, a function of divergence to time near  $x^{0.5}$  will describe unconstrained evolution, a function near  $x^{0.0}$  will describe constrained evolution, and a function of  $x^{1.0}$  will describe directional evolution. Figure 9.15 shows four plots of divergence and time since common ancestry. In the first two, time was measured from the fossil record; in the second two, it was measured as mitochondrial cytochrome *b* genetic distance. A series of functions were fit to each plot with powers of  $x$  varying between 0.1 and 1 (broken lines). The line that minimized the residual error

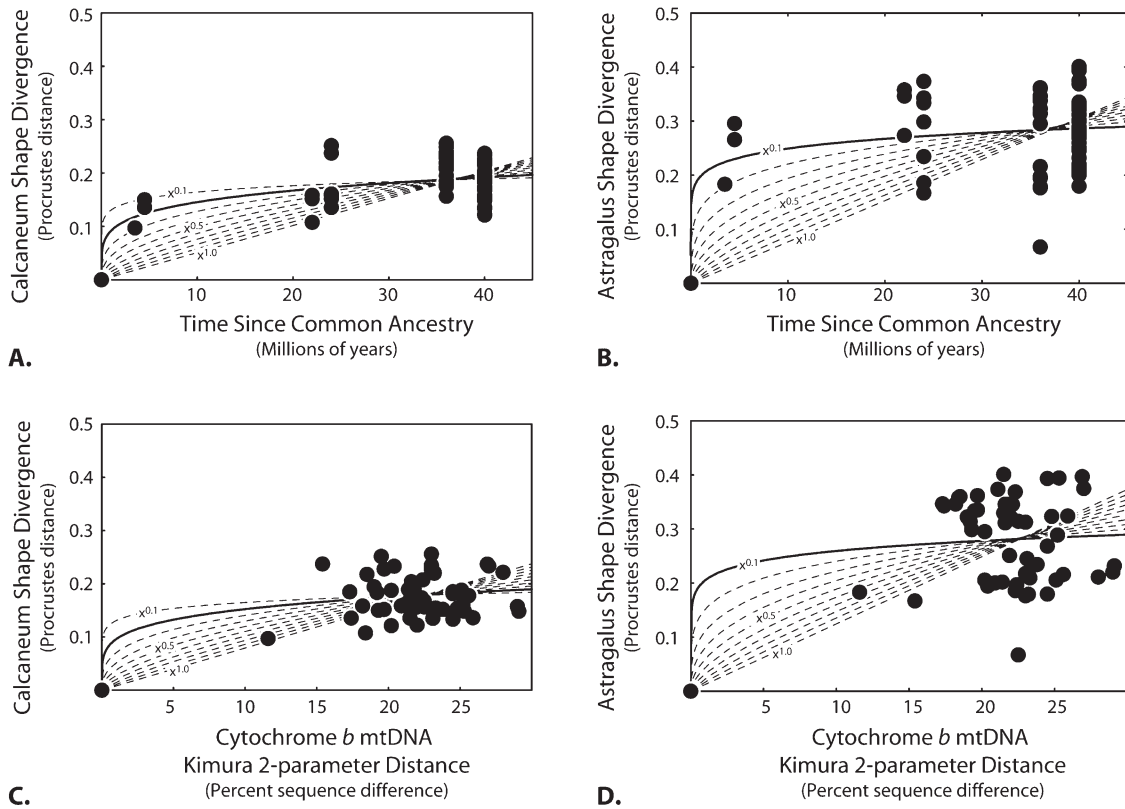


FIGURE 9.15. Mode of evolution in tarsal morphology inferred by fitting functions of  $x$ . A, Calcaneum divergence as a function of time since common ancestry. B, Astragalus divergences as a function of time since common ancestry. C, Calcaneum divergences as a function of genetic distance. D, Astragalus divergence as a function of genetic distance. Ten functions were fit (broken curves) to find the best (solid curve). The best fit for all four was  $x^{0.1}$  or  $x^{0.2}$ , values consistent with the broad constraints characteristic of adaptive zones.

was chosen as the best hypothesis of evolutionary mode. For the calcaneum, the best fit was obtained by  $x^{0.2}$  and for the astragalus  $x^{0.1}$  (solid lines). Both coefficients indicate that divergence was highly constrained, a finding consistent with the phenotypes being trapped within an adaptive zone.

From the perspective of clades evolving within a constrained phenotypic space, Rosen's (1974) characterization of an adaptive zone as a collection of taxa sharing primitive features is nonsensical. All of the taxa here, fissiped and pinniped, have derived morphologies, easily seen in the difference between the shapes of terminal taxa and their subtending nodes. Indeed, the branch distances reported in Table 9.3 demonstrate that *Phoca's* calcaneum is not much more derived than *Ailurus's*. The fissiped taxa cannot be said to be united by symplesiomorphy, because they do not share anything in common that they do not also share with *Phoca*. Rather, fissiped taxa are constrained by the adaptive zone boundaries so that their morphology suffers from considerable convergence (convergence is a better term than homoplasy, because the latter implies identical character states, which do not easily occur in continuously variable quantitative data). Phylogenetically convergent similarity is not shared ancestral similarity. Consequently, the criteria proposed here for recognizing an adaptive zone rather belatedly answer Rosen's (1974) challenge that no evolutionist has been able to

formulate adaptive zone concepts into a "recognizable methodology".

## 9.4 Conclusions

The main functional findings of this study are not new. The significance of the position of the sustentaculum, the length of the peroneal process, the shape of facets, and the length of the astragalus neck for carnivore ankle mobility has been long recognized. Rather, this study contributed a quantitative assessment of the three-dimensional form of these features, allowing direct statistical analysis. This study found, for example, that the long held opinion that intertarsal mobility is enhanced by larger and flatter facets on one of the two bones was not supported in Carnivora. This study also generated new hypotheses about carnivoran tarsal evolution: the reconstructions based on modern taxa predict that the ancestral carnivoran had tarsals adapted for a semidigitigrade terrestrial locomotion and the quantification of the rate of shape change on the phylogenetic tree suggested that pinniped tarsals no faster than in fissiped clades, even though pinniped morphology appears to be more derived.

The more far reaching significance of the paper concerns the relationship between form, function, and phylogeny.

Function and phylogeny are not mutually exclusive explanations for morphological variation. Skeletal morphology is clearly functional and therefore susceptible to convergent selection, a process which confuses phylogenetic interpretation. The carnivoran tarsals in this study are a good example, because their shape is statistically associated with locomotor type, stance, and number of digits and because the regions of shape space associated with these functional categories had been converged upon by unrelated clades. Yet, evolutionary transformations, even convergent ones, occur through phylogenetic divergence, meaning that variance among the most closely related taxa will have a strong phylogenetic component. In this study, young clades, such as the felids, were not affected by convergence even though deeper clades were. Phylogenetic history leaves an imprint on evolving

morphology – the issue for systematics is to determine how the interaction between common ancestry and adaptive convergence affect the dominance of phylogeny and function in morphometric data from a given set of taxa.

Simpson’s adaptive zones provide a suitable analogy for understanding the tradeoffs between common ancestry and functional adaptation. If an adaptive zone is considered to be a region of morphospace whose axes are defined by functionally correlated variation and within whose space evolution is constrained, then the concept can be used to assess the conditions under which phylogeny should be reconstructable. Fissiped tarsals fell within such a region whose boundaries were not normally crossed during the evolution of the group (Figure 9.16). The functional, terrestrial nature of the boundaries of the morphospace can be clearly seen in the morphologies that

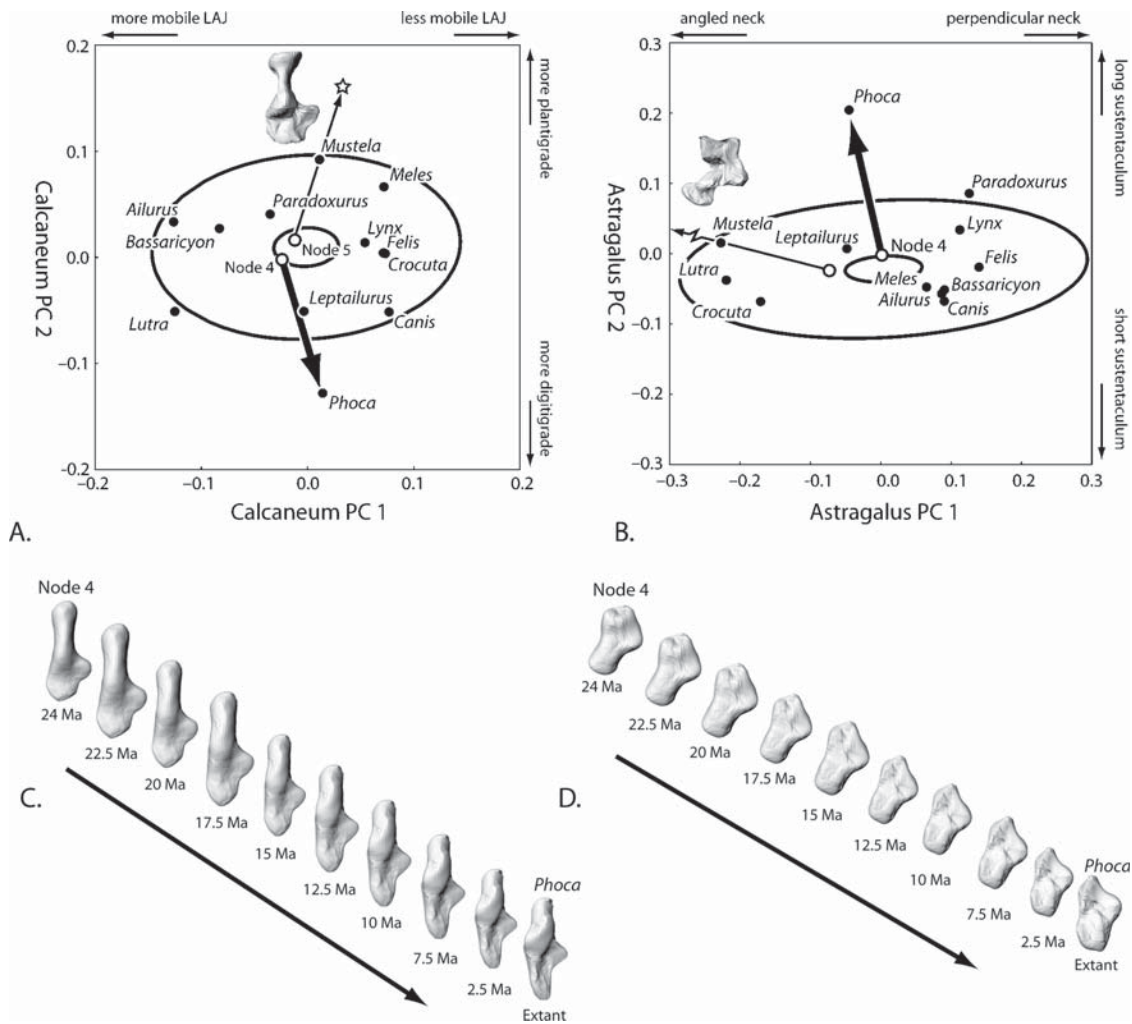


FIGURE 9.16. Escape from the Fissiped adaptive zone. A, Calcaneum adaptive zone projected onto the first two PCs. Ellipses characterizing the adaptive zone are the 5th and 95th percentiles of fissiped shape variation. The heavy arrow shows the branch leading from Node 4 to *Phoca*, which is modeled in C. The light arrow shows a hypothetical trajectory from Node 5 to a point outside the adaptive zone (star) with *Mustela* as its midpoint. The shape at the hypothetical point is shown. B, Astragalus adaptive zone with the same conventions. Note the hypothetical point beyond *Mustela* lies outside the graph area. C, Calcaneum shape models along the branch leading from Node 4 to *Phoca*, the most probable trajectory for the escape. D, Astragalus shape models for the same branch. The trajectories are shown as dark arrows in A and B.

lie outside them. For example, when the phylogenetic branch leading to *Mustela* is projected outside the zone boundary, the resulting morphology has a combination of features that are functionally incompatible with terrestrial locomotion. That morphology has a broad distal end, but no peroneal tubercle; its sustentacular and calcaneoastagal facets are oriented like a digitigrade terrestrial species, even though these normally have narrow distal calcanea; and its astragalar neck is thin and sharply angled. The branch leading to *Phoca* also traces morphologies that are incompatible with terrestrial locomotion – something known from both visual inspection of the bones and knowledge of movement in living seals. The elongation of the calcaneum facets combined with the enlargement of the astragalus neck and sustentacular facet correspond to a side-to-side movement in the LAJ that undesirable for stable movements on a firm substrate.

If prevalent, adaptive zones like the fissiped one may place identifiable constraints on morphological phylogeny reconstruction. The adaptive zone identified here acts as a loosely constrained Ornstein-Uhlenbeck process, which by erasing deep phylogenetic history as different lineages explore the same morphospace again and again, violates the Brownian motion assumptions required for effective phylogeny reconstruction (Felsenstein, 1988, 2002). The departure of *Phoca* from the adaptive zone further confounds the phylogenetic picture by creating a long-branch that does not easily link to taxa within the zone.

While these findings sound pessimistic in regards to the reconstruction of phylogeny from tarsal morphology, echoing Nadal-Roberts and Collard (2005), such reconstruction is possible in the right circumstances. The limits on reconstruction depend on the size of the adaptive zone, the rate of evolution, and the recency of common ancestry. In the fissiped zone, rate and zone size dictate that the best reconstructions will be with taxa who shared a common ancestor within the previous 5–15 million years, as shown by the position of the felid tarsals and the age of their common ancestor. Thus, we can expect good phylogenetic signal, for example, from living taxa that have radiated since the end of the Miocene, as well as for fossil taxa that radiated within the Early Oligocene. Relationships among taxa whose last common ancestor is older than 5–15 million years could, in principle, be reconstructed if fossils of intermediate ages were strategically included in the analysis, an idea that invites further investigation. The limit for phylogeny reconstruction of 5–15 million years is unlikely to hold across taxa or character complexes, though it is compatible with findings from teeth, mandibles, and skulls in rodents (Caumul and Polly, 2005). Sweeping statements about the lack of phylogenetic signal in morphometric data cannot be expected to hold at all levels of analysis; rather the nature of functional and phylogenetic components of morphological variance need to be scientifically assessed.

*Acknowledgments.* Thanks to Eric Sargis and Marian Dagosto for organizing this volume and allowing my contribution. Annalisa Berta, Andrea Cardini, Alistair Evans, Joseph Felsenstein, Jason Head, Paula Jenkins, Jukka Jernvall, Lauren Morris, Marcelo Sánchez-Villagra, Fred Szalay, Heidi Schutz, Rebecca Spang, Mark Uhen, Blaire Van Valkenburgh, Vera Weisbecker, and two anonymous reviewers provided information, discussed issues, or made comments that contributed to this paper. Norman MacLeod deserves special acknowledgment for lengthy discussions that culminated in the method of placing points on three-dimensional surfaces, discussions without which the 3D surface analysis would not have been possible. Steve Le Comber, and, by extension, George Gamow, made a creative contribution to the measure of joint surface curvature. Andy Currant (NHM) and Haidee Price-Thomas (QMUL) provided access to specimens in their care. Thank you Fred Szalay for always being challenging, controversial, interesting, inspiring, and, more recently, a friend.

## References

- Acerro, A., Tavera, J. J., Reyes, J., 2005. Systematics of the genus *Bagre* (Siluriformes: Ariidae): a morphometric approach. *Cybium* 29, 127–133.
- Alexander, R. M., 2003. Principles of Animal Locomotion. Princeton University Press, Princeton, NJ.
- Alroy, J., 1998. Cope's rule and the dynamics of body mass evolution in North American fossil mammals. *Science* 280, 731–734.
- Arnold, S. J., Pfrender, M. E., Jones, A. G., 2001. The adaptive landscape as a conceptual bridge between micro- and macroevolution. *Genetica* 112–113, 9–32.
- Bininda-Emonds, O. R. P., Gittleman, J. L., 2000. Are pinnipeds functionally different from fissiped carnivores? The importance of phylogenetic comparative analyses. *Evolution* 54, 1011–1023.
- Bininda-Emonds, O. R. P., Gittleman, J. L., Purvis, A., 1999. Building large trees by combining phylogenetic information: a complete phylogeny of the Carnivora (Mammalia). *Biological Reviews of the Cambridge Philosophical Society* 74, 143–175.
- Bock, W. J., 1965. The role of adaptive mechanisms in the origin of higher levels of organization. *Systematic Zoology* 14, 272–287.
- Bock, W. J., von Wahlert, G., 1965. Adaptation and the form-function complex. *Evolution* 19, 269–299.
- Bookstein, F. L., 1991. Morphometric Tools for Landmark Data. Cambridge University Press, Cambridge.
- Bookstein, F. L., Gingerich, P. D., Kluge, A. G., 1978. Hierarchical linear modeling of the tempo and mode of evolution. *Paleobiology* 4, 120–134.
- Brown, W. M., George, M. Jr., Wilson, A. C., 1979. Rapid evolution of animal mitochondrial DNA. *Proceedings of the National Academy of Sciences USA* 76, 1967–1971.
- Butler, M. A., King, A. A., 2004. Phylogenetic comparative analysis: a modeling approach for adaptive evolution. *American Naturalist* 164, 683–695.
- Caumul, R., Polly, P. D. 2005. Comparative phylogenetic and environmental components of morphological variation: skull, mandible and molar shape in marmots (*Marmota*, Rodentia). *Evolution* 59.

- Cheverud, J. M., 1996. Developmental integration and the evolution of pleiotropy. *American Zoologist* 36, 44–50.
- Clevedon Brown, J., Yalden, D. W., 1973. The description of mammals -2. Limbs and locomotion of terrestrial mammals. *Mammal Review* 3, 107–135.
- Cock, A. G., 1966. Genetical aspects of metrical growth and form in animals. *Quarterly Review of Biology* 41, 131–190.
- Davis, C. S., Delisle, I., Stirling, I., Siniff, D. B., Strobeck, C., 2004. A phylogeny of the extant Phocidae inferred from complete mitochondrial DNA coding regions. *Molecular Phylogenetics and Evolution* 33, 363–377.
- Decker, R. L., Szalay, F. S., 1974. Origins and function of the pes in the Eocene Adapidae (Lemuriformes, Primates). In: Jenkins, F. A., Jr. (Ed.), *Primate Locomotion*. Academic Press, New York, pp. 261–291.
- Dryden, I. L., Mardia, K. V., 1998. *Statistical Analysis of Shape*. Wiley, New York.
- Eguchi, S., Townsend, G. C., Richards, L. C., Hughes, T., Kasai, K., 2004. Genetic contribution to dental arch size variation in Australian twins. *Archives of Oral Biology* 49, 1015–1024.
- Eisenberg, J. F., 1981. *The Mammalian Radiations: An Analysis of Trends in Evolution, Adaptation, and Behavior*. Chicago University Press, Chicago, IL.
- Eisenberg, J. F., 1989. *Mammals of the Neotropics: the Northern Neotropics*. University of Chicago Press, Chicago, IL.
- Evans, H. E., 1993. *Miller's Anatomy of the Dog*, 3rd Ed. W. B. Saunders, Philadelphia.
- Felsenstein, J., 1973. Maximum-likelihood estimation of evolutionary trees from continuous characters. *American Journal of Human Genetics* 25, 471–492.
- Felsenstein, J., 1981. Evolutionary trees from gene frequencies and quantitative characters: finding maximum likelihood estimates. *Evolution* 35, 1229–1242.
- Felsenstein, J., 1988. Phylogenies and quantitative characters. *Annual Review of Ecology and Systematics* 19, 445–471.
- Felsenstein, J., 1993. PHYLIP Phylogeny Inference Package version 3.5c. Distributed by the author. Department of Genetics, University of Washington, Seattle.
- Felsenstein, J., 2002. Quantitative characters, phylogenies, and morphometrics. In: MacLeod, N., Forey, P. (Eds.), *Morphology, Shape, and Phylogenetics*. Taylor & Francis, London, pp. 27–44.
- Flynn, J. J., 1996. Carnivoran phylogeny and rates of evolution: morphological, taxic, and molecular. In: Gittleman, J. L. (Ed.), *Carnivore Behavior, Ecology, and Evolution*, Cornell University Press, Ithaca, NY, pp. 542–581.
- Flynn, J. J., Nedbal, M. A., 1998. Phylogeny of the Carnivora (Mammalia): congruence vs. incompatibility among multiple data sets. *Molecular Phylogenetics and Evolution* 9, 414–426.
- Flynn, J. J., Wesley-Hunt, G. D., 2005. Carnivora. In: Archibald, D., Rose, K. (Eds.), *Origin, Timing, and Relationships of the Major Clades of Extant Placental Mammals*. Johns Hopkins University Press, Baltimore, MD, pp. 175–198.
- Flynn, J. J., Neff, N. A., Tedford, R. H., 1988. Phylogeny of the Carnivora. In: Benton, M. J. (Ed.), *The Phylogeny and Classification of Tetrapods*, Volume 2. Clarendon, Oxford, pp. 73–116.
- Flynn, J. J., Nedbal, M. A., Dragoo, J. W., Honeycutt, R. L., 2000. Whence the red panda? *Molecular Phylogenetics and Evolution* 17, 190–199.
- Flynn, J. J., Finarelli, J. A., Zehr, S., Hsu, J., Nedbal, M. A., 2005. Molecular phylogeny of the Carnivora Mammalia: assessing the impact of increased sampling on resolving enigmatic relationships. *Systematic Biology* 54, 317–337.
- Fox, R. C., Youzwshyn, G. P., 1994. New primitive carnivorans Mammalia from the Paleocene of Western Canada, and their bearing on relationships of the order. *Journal of Vertebrate Paleontology* 14, 382–404.
- Gambaryan, P. P., 1974. *How Mammals Run: Anatomical Adaptations*. Wiley, New York.
- Garland, T. Jr., Ives, A. R., 2000. Using the past to predict the present: confidence intervals for regression equations in phylogenetic comparative methods. *American Naturalist* 155, 346–364.
- Garland, T. Jr., Midford, P. E., Ives, A. R., 1999. An introduction to phylogenetically based statistical methods, with a new method for confidence intervals on ancestral values. *American Zoologist* 39, 374–388.
- Gaubert, P., Veron, G., 2003. Exhaustive sample set among Viverridae reveals the sister-group of felids: the linsangs as a case of extreme morphological convergence within Feliformia. *Proceedings of the Royal Society of London B* 270, 2523–2530.
- Gingerich, P. D., 1993. Quantification and comparison of evolutionary rates. *American Journal of Science* 293-A, 453–478.
- Gingerich, P. D., 2001. Rates of evolution on the time scale of the evolutionary process. *Genetica* 112–113, 127–144.
- Gingerich, P. D., Winkler, D. A., 1985. Systematics of Paleocene Viverridae (Mammalia, Carnivora) in the Bighorn Basin and Clark's Fork Basin, Wyoming. *Contributions from the Museum of Paleontology, University of Michigan* 27, 87–128.
- Grafen, A., 1989. The phylogenetic regression. *Philosophical Transactions of the Royal Society of London B* 326, 119–137.
- Graur, D., Martin, W., 2004. Reading the entrails of chickens: molecular timescales of evolution and the illusion of precision. *Trends in Genetics* 20, 80–86.
- Gonyea, W. J., 1976. Adaptive differences in the body proportions of large felids. *Acta Anatomica* 96, 81–96.
- Goslow, G. E., Van de Graff, K., 1982. Hindlimb joint angle changes and action of the primary extensor muscles during posture and locomotion in the Striped skunk *Mephitis mephitis*. *Journal of Zoology (London)* 1982, 405–419.
- Greene, E. C., 1935. Anatomy of the rat. *Transactions of the American Philosophical Society* 27, 1–370.
- Gregory, W. K., 1951. *Evolution Emerging*. Macmillan, New York.
- Grüneberg, H., 1967. *The Pathology of Development: A Study of Inherited Skeletal Disorders in Animals*. Blackwell, Oxford.
- Hansen, T. F., Martins, E. P., 1996. Translating between microevolutionary process and macroevolutionary patterns: the correlation structure of interspecific data. *Evolution* 50, 1404–1417.
- Hecht, M. K., 1965. The role of natural selection and evolutionary rates in the origin of higher levels of organization. *Systematic Zoology* 14, 301–317.
- Heinrich, R. E., Rose, K. D., 1997. Postcranial morphology and locomotor behaviour of two early Eocene miacoid carnivorans, *Vulpavus* and *Didymictis*. *Palaeontology* 40, 279–305.
- Hildebrand, M., 1954. Comparative morphology of the body skeleton in recent Canidae. University of California Publications in Zoology 52, 399–470.
- Hildebrand, M., 1980. The adaptive significance of tetrapod gait selection. *American Zoologist* 20, 255–267.

- Howard, L. D., 1973. Muscular anatomy of the hind limb of the otter *Enhydra lutris*. *Proceedings of the California Academy of Sciences* 40, 335–416.
- Howell, A. B., 1929. Contribution to the comparative anatomy of the eared and earless seals genera *Zalophus* and *Phoca*. *Proceedings of USNM* 73, 1–142.
- Howell, A. B., 1930. *Aquatic Mammals: Their Adaptations to Life in the Water*. Charles Thomas, Springfield, IL.
- Howell, A. B., 1944. *Speed in Animals*. University of Chicago Press, Chicago, IL.
- Hunt, R. M., Tedford, R. A., 1993. Phylogenetic relationships within the aeluroid carnivora and implications of their temporal and geographic distribution. In: Szalay, F. S., Novacek, M. J., McKenna (Eds.), *Mammalian Phylogeny: Placentals*. Springer, New York, pp. 53–73.
- Janis, C. M., Baskin, J. A., Berta, A., Flynn, J. J., Gunnell, G. F., Hunt, R. M., Martin, L. D., Munthe, K., 1998. Carnivorous mammals. In: Janis, C. M., Scott, K. M., Jacobs, L. J. (Eds.), *Tertiary Mammals of North America*. Cambridge University Press, Cambridge, pp. 73–90.
- Jenkins, F. A., Camazine, S. M., 1977. Hip structure and locomotion in ambulatory and cursorial carnivores. *Journal of Zoology (London)* 181, 351–370.
- Jenkins, F. A., McClearn, D., 1984. Mechanisms of hind foot reversal in climbing mammals. *Journal of Morphology* 182, 197–219.
- Kennel Club, 1998. *Illustrated Breed Standards: the Official Guide to Registered Breeds*. Ebury, London.
- Kimura, M., 1980. A simple method for estimating evolutionary rates of base substitutions through comparative studies of nucleotide-sequences. *Journal of Molecular Evolution* 16, 111–120.
- King, J. E., 1966. Relationships of the hooded and elephant seals (Genera *Cystophora* and *Mirounga*). *Journal of Zoology (London)* 148, 385–398.
- Kirkpatrick, M., 1982. Quantum evolution and punctuated equilibria in continuous genetic characters. *American Naturalist* 119, 833–848.
- Kluge, A. G., 1989. A concern for evidence and a phylogenetic hypothesis of relationships among *Epicrates* (Boidae, Serpentes). *Systematic Zoology* 38, 7–25.
- Koepfli, K.-P., Wayne, R. K., 1998. Phylogenetic relationships of otters Carnivora: Mustelidae based on mitochondrial cytochrome b sequences. *Journal of Zoology* 246, 401–416.
- Koepfli, K.-P., Wayne, R. K., 2003. Type-1 STS markers are more informative than cytochrome b in phylogenetic reconstruction of the Mustelidae (Mammalia: Carnivora). *Systematic Biology* 52, 571–593.
- Lande, R., 1976. Natural selection and random genetic drift in phenotypic evolution. *Evolution* 30, 314–344.
- Lande, R., 1986. The dynamics of peak shifts and the pattern of morphological evolution. *Paleobiology* 12, 343–354.
- Ledge, C., Arnason, Ú., 1996a. Phylogenetic analyses of complete cytochrome b genes of the Order Carnivora with particular emphasis on the Canifonia. *Journal of Molecular Evolution* 42, 135–144.
- Ledge, C., Arnason, Ú., 1996b. Phylogenetic relationships within caniform carnivores based on analyses of the mitochondrial 12S rRNA gene. *Journal of Molecular Evolution* 43, 641–649.
- Lento, G. M., Hickson, R. E., Chambers, G. K., Penny, D., 1995. Use of spectral analysis to test hypotheses on the origin of pinnipeds. *Molecular Biology and Evolution* 12, 28–52.
- Lewis, O. J., 1989. *Functional Morphology of the Evolving Hand and Foot*. Clarendon, Oxford.
- Lohmann, G. P., 1983. Eigenshape analysis of microfossils: a general morphometric method for describing changes in shape. *Mathematical Geology* 15, 659–672.
- Lohmann, G. P., Schweitzer, P. N., 1990. On eigenshape analysis. The University of Michigan Museum of Zoology, Special Publication 2, 145–166.
- MacConaill, M. A., 1946a. Studies in the mechanics of synovial joints. I. Fundamental principles and diadochal movements. *Irish Journal of Medical Science* 246, 190–199.
- MacConaill, M. A., 1946b. Studies in the mechanics of synovial joints. II. Displacements on articular surfaces and the significance of saddle joints. *Irish Journal Medical Science* 247, 223–235.
- MacConaill, M. A., 1946c. Studies in the mechanics of synovial joints. III. Hinge-joints and the nature of intra-articular displacements. *Irish Journal of Medical Science* 249, 620–626.
- MacLeod, N., 1999. Generalizing and extending the eigenshape method of shape space visualization and analysis. *Paleobiology* 25, 107–138.
- MacLeod, N., 2002. Testing evolutionary hypotheses with adaptive landscapes: use of random phylogenetic-morphological simulation studies. *Mathematical Geology* 6, 45–55.
- MacLeod, N., Rose, K. D., 1993. Inferring locomotor behavior in paleogene mammals via eigenshape analysis. *American Journal of Science* 293-A, 300–355.
- Martins, E. P., Hansen, T. F., 1997. Phylogenies and the comparative method: a general approach to incorporating phylogenetic information into the analysis of interspecific data. *American Naturalist* 149, 646–667.
- McArdle, B., Rodrigo, A. G., 1994. Estimating the ancestral states of a continuous-valued character using squared-change parsimony: an analytical solution. *Systematic Biology* 43, 573–578.
- Miyamoto, M. M., 1985. Consensus cladograms and general classifications. *Cladistics* 1, 186–189.
- Nadal-Roberts, M., Collard, M., 2005. The impact of methodological choices on assessments of the reliability of fossil primate phylogenetic hypotheses. *Folia Primatologica* 76, 207–221.
- Nei, M., 1987. *Molecular Evolutionary Genetics*. Columbia University Press, New York.
- Pie, M. R., Weitz, J. S., 2005. A null model of morphospace occupation. *American Naturalist* 166, E1–E13.
- Polly, P. D., 1997. Ancestry and species definition in paleontology: a stratocladistic analysis of Viverravidae (Carnivora, Mammalia) from Wyoming. *Contributions from the Museum of Paleontology, University of Michigan* 30, 1–53.
- Polly, P. D., 1998. Cope's Rule. *Science* 282, 50–51.
- Polly, P. D., 2001. Paleontology and the comparative method: ancestral node reconstructions versus observed node values. *American Naturalist* 157, 596–609.
- Polly, P. D., 2002. Phylogenetic tests for differences in shape and the importance of divergence times: Eldredge's enigma explored. In: MacLeod, N., Forey, P. (Eds.), *Morphology, Shape, and Phylogenetics*. Taylor & Francis, London, pp. 220–246.
- Polly, P. D., 2003a. Paleophylogeography: the tempo of geographic differentiation in marmots (*Marmota*). *Journal of Mammalogy* 84, 369–384.
- Polly, P. D., 2003b. Paleophylogeography of *Sorex araneus*: molar shape as a morphological marker for fossil shrews. *Mammalia* 68, 233–243.

- Polly, P. D., 2004. On the simulation of the evolution of morphological shape: multivariate shape under selection and drift. *Palaeontologia Electronica* 7.2.7A, 28pp. [http://palaeo-electronica.org/paleo/2004\\_2/evo/issue2\\_04.htm](http://palaeo-electronica.org/paleo/2004_2/evo/issue2_04.htm)
- Polly, P. D., 2005. Development, geography, and sample size in P matrix evolution: molar-shape change in island populations of *Sorex araneus*. *Evolution and Development* 7, 29–41.
- Rohlf, F. J., 1990. Rotational fit Procrustes methods. In: Rohlf, F. J., Bookstein, F. L. (Eds.), *Proceedings of the Michigan Morphometrics Workshop*. The University of Michigan Museum of Zoology, Special Publication 2, 227–236.
- Rohlf, F. J., 2001. Comparative methods for the analysis of continuous variables: geometric interpretations. *Evolution* 55, 2143–2160.
- Rohlf, F. J., Corti, M., 2000. Use of two-block partial least-squares to study covariation in shape. *Systematic Biology* 49, 740–753.
- Rohlf, F. J., Slice, D., 1990. Extensions of the Procrustes method for the optimal superimposition of landmarks. *Systematic Zoology* 39, 40–49.
- Roopnarine, P. D., 2001. The description and classification of evolutionary mode: a computational approach. *Paleobiology* 27, 446–465.
- Rosen, D. E., 1974. Cladism or gradism? A reply to Ernst Mayr. *Systematic Zoology* 23, 446–451.
- Salton, J. A., Szalay, F. S., 2004. The tarsal complex of Afro-malagasy Tenrecoidea: a search for phylogenetically meaningful characters. *Journal of Mammalian Evolution* 11, 73–104.
- Salazar-Ciudad, I., Jernvall, J., 2004. How different types of pattern formation mechanisms affect the evolution of form and development. *Evolution and Development* 6, 6–16.
- Sampson, P. D., Streissguth, A. P., Barr, H. M., Bookstein, F. L., 1989. Neurobehavioral effects of prenatal alcohol: Part II. Partial least squares analysis. *Neurotoxicology and Teratology* 11, 477–491.
- Sato, J. J., Hosoda, T., Wolsan, M., Tsuchiya, K., Yamamoto, Y., Suzuki, H., 2003. Phylogenetic relationship and divergence times among mustelids Mammalia: Carnivora based on nucleotide sequences of the nuclear interphotoreceptor retinoid binding protein and mitochondrial cytochrome b genes. *Zoological Science* 20, 243–264.
- Sato, J. J., Hosoda, T., Wolsan, M., Suzuki, H., 2004. Molecular phylogeny of *Arctoides* (Mammalia: Carnivora) with emphasis on phylogenetic and taxonomic positions of the ferret-badgers and skunks. *Zoological Science* 21, 111–118.
- Schaeffer, B., 1947. Notes on the origin and function of the artiodactyl tarsus. *American Museum Novitates* 1356, 1–24.
- Schluter, D., 1996. Adaptive radiation along genetic lines of least resistance. *Evolution* 50, 1766–1774.
- Schmalhausen, I. I., 1949. *Factors of Evolution: The Theory of Stabilizing Selection*. Translated by T. Dobzhansky. Blakiston, Philadelphia.
- Silva, M., Downing, J. A., 1995. *The CRC Handbook of Mammalian Body Masses*. CRC, Boca Raton, FL.
- Simpson, G. G., 1944. *Tempo and Mode in Evolution*. Columbia University Press, New York.
- Simpson, G. G., 1945. The principles of classification and a classification of mammals. *Bulletin of the AMNH* 85, 1–350.
- Simpson, G. G., 1953. *The Major Features of Evolution*. Columbia University Press, New York.
- Slattery, J. P., O'Brien, S. J., 1995. Molecular phylogeny of the red panda *Ailurus fulgens*. *Heredity* 86, 413–422.
- Springer, M. S., 1997. Molecular clocks and the timing of placental and marsupial radiations in relation to the Cretaceous-Tertiary boundary. *Journal of Mammalian Evolution* 4, 285–302.
- Stanley, S. M., 1973. Explanation for Cope's rule. *Evolution* 27, 1–26.
- Szalay, F. S., 1977a. Phylogenetic relationships and a classification of the eutherian Mammalia. In: Hecht, M. K., Goody, P. C., Hecht, B. M. (Eds.), *Major Patterns in Vertebrate Evolution*. Plenum, New York, pp. 315–374.
- Szalay, F. S., 1977b. Ancestors, descendants, sister groups, and testing of phylogenetic hypotheses. *Systematic Zoology* 26, 12–18.
- Szalay, F. S., 1981. Functional analysis and the practice of the phylogenetic method as reflected by some mammalian studies. *American Zoologist* 21, 37–45.
- Szalay, F. S., 1984. Arboreality: is it homologous in Metatherian and Eutherian mammals? In: Hecht, M. K., Wallace, B., Prance, G. T. (Eds.), *Evolutionary Biology*, Volume 18. Plenum, New York.
- Szalay, F. S., 1994. *Evolutionary History of the Marsupials and an Analysis of Osteological Characters*. Cambridge University Press, Cambridge.
- Szalay, F. S., 2000. Function and adaptation in paleontology and phylogenetics: Why do we omit Darwin? *Palaeontologia Electronica* 3.2.2, 25 pp. 372KB. [http://palaeo-electronica.org/2000\\_2/darwin/issue2\\_00.htm](http://palaeo-electronica.org/2000_2/darwin/issue2_00.htm)
- Szalay, F. S., Bock, W. J., 1991. Evolutionary theory and systematics: relationships between process and patterns. *Zeitschrift für Zoologische Systematik und Evolutionsforschung* 29, 1–39.
- Szalay, F. S., Decker, R. L., 1974. Origins, evolution, and function of the tarsus in Late Cretaceous Eutheria and Paleocene Primates. In: Jenkins, F. A., Jr. (Ed.), *Primate Locomotion*. Academic Press: New York, pp. 223–259.
- Szalay, F. S., Drawhorn, G., 1980. Evolution and diversification of the Archona in an arboreal milieu. In: Luckett, W. P. (Ed.), *Comparative Biology and Evolutionary Relationships of Tree Shrews*. Plenum, New York, pp. 133–169.
- Szalay, F. S., Schrenk, F., 1998. The middle Eocene Eurotamandua and a Darwinian phylogenetic analysis of “edentates.” *Kaupia* 7, 97–186.
- Taylor, M. E., 1970. Locomotion in some East African viverrids. *Journal of Mammals* 51, 42–51.
- Taylor, M. E., 1976. The functional anatomy of the hindlimb of some African Viverridae (Carnivora). *Journal of Morphology* 148, 227–254.
- Taylor, M. E., 1988. Foot structure and phylogeny in the Viverridae (Carnivora). *Journal of Zoology (London)* 216, 131–139.
- Taylor, M. E., 1989. Locomotor adaptations. In: Gittleman, J. L. (Ed.), *Carnivore Behavior, Ecology, and Evolution*. Cornell University Press, Ithaca, NY, pp. 382–409.
- Thompson, J. D., Gibson, T. J., Plewniak, F., Jeanmougin, F., Higgins, D. G., 1997. The ClustalX windows interface: flexible strategies for multiple sequence alignment aided by quality analysis tools. *Nucleic Acids Research* 24, 4876–4882.
- Thorpe, R. S., 1981. The morphometrics of the mouse: a review. In: Berry, R. J. (Ed.), *Biology of the House Mouse*. Zoological Society of London, London, pp. 85–125.
- Van Valkenburgh, B., 1985. Locomotor diversity within past and present guilds of large predatory mammals. *Journal of Vertebrate Paleontology* 11, 406–428.

- Van Valkenburgh, B., Wang, X. M., Damuth, J., 2004. Cope's rule, hypercarnivory, and extinction in North American canids. *Science* 306, 101–104.
- Veron, G., Heard, S., 2000. Molecular systematics of the Asiatic Viverridae Carnivora inferred from mitochondrial cytochrome b sequence analysis. *Journal of Zoological Systematics and Evolutionary Research* 38, 209–217.
- Veron, G., Colyn, M., Dunham, A. E., Taylor, P., Gaubert, P., 2004. Molecular systematics and evolution of sociality in mongooses Herpestidae, Carnivora. *Molecular Phylogenetics and Evolution* 30, 582–598.
- Wake, D. B., Roth, G., Wake, M. H., 1983. On the problem of stasis in organismal evolution. *Journal of Theoretical Biology* 101, 211–224.
- Wang, X., 1997. New cranial material of *Simocyon* from China and its implications for phylogenetic relationships to the Red panda *Ailurus*. *Journal of Vertebrate Paleontology* 17, 184–198.
- Wayne, R. K., Benveniste, R. E., Janczewski, D. N., O'Brien, S. J., 1989. Molecular and biochemical evolution of the Carnivora. In: Gittleman, J. L. (Ed.), *Carnivore Behavior, Ecology, and Evolution*, Volume 1. Comstock Cornell, Ithaca, NY, pp. 465–495.
- Werdelin, L., 1996. Carnivoran ecomorphology: a phylogenetic perspective. In: Gittleman, J. L. (Ed.), *Carnivore Behavior, Ecology, and Evolution*, Volume 2. Comstock Cornell, Ithaca, NY, pp. 582–624.
- Wesley-Hunt, G. D., Flynn, J. J., 2005. Phylogeny of the carnivora: basal relationships among the carnivoramorphan and assessment of the position of "Miacoidae" relative to crown-clade Carnivora. *Journal of Systematic Palaeontology* 3, 1–28.
- Wolsan, M., 1993. Phylogeny and classification of early European Mustelida (Mammalia: Carnivora). *Acta Theriologica* 38, 345–384.
- Wozencraft, W. C., 1989. The phylogeny of the recent Carnivora. In: Gittleman, J. L. (Ed.), *Carnivore Behavior, Ecology, and Evolution*, Volume 1. Comstock Cornell, Ithaca, NY, pp. 495–535.
- Wright, S., 1988. Surfaces of selective value revisited. *American Naturalist* 131, 115–123.
- Wyss, A. R., 1988. On "retrogression" in the evolution of the Phocinae and phylogenetic affinities of the monk seals. *American Museum Novitates* 2924, 1–38.
- Wyss, A. R., Flynn, J. J., 1993. A phylogenetic analysis and definition of the Carnivora. In: Szalay, F. S., Novacek, M. J., McKenna, M. C. (Eds.), *Mammal Phylogeny: Placentals*. Springer, New York, pp. 32–52.
- Yu, L., Zhang, Y.-P., 2005. Phylogenetic studies of pantherine cats (Felidae) based on multiple genes, with novel application of nuclear  $\beta$ -fibrinogen intron 7 to carnivores. *Molecular Phylogenetics and Evolution* 35, 483–495.
- Yu, L., Li, Q.-W., Ryder, O. A., Zhang, Y.-P., 2004. Phylogenetic relationships within mammalian order Carnivora indicated by sequences of two nuclear DNA genes. *Molecular Phylogenetics and Evolution* 33, 694–705.
- Zelditch, M. L., Ludrigan, B. L., Garland, T., 2004. Developmental regulation of skull morphology. I. Ontogenetic dynamics of variance. *Evolution and Development* 6, 194–206.